

# Aneuploidy can be an evolutionary diversion on the path to adaptation

Ilia Kohanovski<sup>a,b,1</sup>, Martin Pontz<sup>a,1</sup>, Pétra Vande Zande<sup>c</sup>, Anna Selmecki<sup>c</sup>, Orna  
Dahan<sup>d</sup>, Yitzhak Pilpel<sup>d</sup>, Avihu H. Yona<sup>e</sup>, and Yoav Ram<sup>a,\*</sup>

<sup>a</sup>School of Zoology, Faculty of Life Sciences, Tel Aviv University, Tel Aviv, Israel

<sup>b</sup>School of Computer Science, Reichman University, Herzliya, Israel

<sup>c</sup>Department of Microbiology and Immunology, University of Minnesota Medical School, Minneapolis, MN

<sup>d</sup>Department of Molecular Genetics, Weizmann Institute of Science, Rehovot, Israel

<sup>e</sup>Institute of Biochemistry, Food Science and Nutrition, Robert H. Smith Faculty of Agriculture, Food and  
Environment, The Hebrew University of Jerusalem, Israel

<sup>1</sup>These authors contributed equally to this work

\*Corresponding author: yoav@yoavram.com

January 11, 2024

Classifications. Biological Sciences: Evolution, Genetics, Microbiology, Population Biology.

Keywords: whole-chromosome duplication, evolutionary model, adaptive evolution

**Abstract**

Aneuploidy is common in eukaryotes, often leading to decreased fitness. However, evidence from fungi and human tumour cells suggests that specific aneuploidies can be beneficial under stressful conditions and facilitate adaptation. In a previous evolutionary experiment with yeast, populations evolving under heat stress became aneuploid, only to later revert to euploidy after beneficial mutations accumulated. It was therefore suggested that aneuploidy is a "stepping stone" on the path to adaptation. Here, we test this hypothesis. We use Bayesian inference to fit an evolutionary model with both aneuploidy and mutation the experimental results. We then predict the genotype frequency dynamics during the experiment, demonstrating that most of the evolved euploid population likely did not descend from aneuploid cells, but rather from the euploid wildtype population. Our model shows how the beneficial mutation supply—the product of population size and beneficial mutation rate—determines the evolutionary dynamics: with low supply, much of the evolved population descends from aneuploid cells; but with high supply, beneficial mutations are generated fast enough to outcompete aneuploidy due to its inherent fitness cost. Our results suggest that despite its potential fitness benefits under stress, aneuploidy can be an evolutionary "detour" rather than a "stepping stone": it can delay, rather than facilitate, the adaptation of the population, and cells that become aneuploid may leave less descendants compared to cells that remain diploid.

## 34 Introduction

Aneuploidy is an imbalance in the number of chromosomes in the cell: an incorrect karyotype.  
36 Evidence suggests aneuploidy is very common in eukaryotes, e.g. animals<sup>49,38,2</sup>, and fungi<sup>41,73,45,62</sup>.  
Aneuploidy has been implicated in cancer formation, progression, and drug resistance<sup>4,51,49,48,23,34</sup>.  
38 It is also common in protozoan pathogens of the *Leishmania* genus, a major global health concern<sup>36</sup>,  
and contributes to the emergence of drug resistance<sup>52</sup> and virulence<sup>37</sup> in fungal pathogens, which  
40 are under-studied<sup>47</sup>, despite infecting a billion people per year, causing significant morbidity in >150  
million and death in >1.5 million people per year<sup>52,47</sup>.  
42 Experiments with human and mouse embryos found that most germ-line aneuploidies are lethal. Ane-  
uploidies are also associated with developmental defects and lethality in other multicellular organ-  
44 isms<sup>55</sup>. For example, aneuploid mouse embryonic cells grow slower than euploid cells<sup>67</sup>. Similarly,  
in unicellular eukaryotes growing in benign conditions, aneuploidy usually leads to slower growth and  
46 decreased overall fitness, in part due to proteotoxic stress due to increased expression, gene dosage  
imbalance, and hypo-osmotic-like stress<sup>39,65,41,55,50,27,72,66,68,46</sup>.  
48 However, aneuploidy can be beneficial under stressful conditions due to the wide range of phenotypes  
it can produce, some of which are advantageous<sup>41,68</sup>. Indeed, in a survey of 1,011 yeast strains,  
50 aneuploidy has been detected in about 19%<sup>42</sup>. Thus, aneuploidy can lead to rapid adaptation in  
unicellular eukaryotes<sup>17,64,21,44</sup>, as well as to rapid growth of somatic tumour cells<sup>51,57</sup>. For example,  
52 aneuploidy in *Saccharomyces cerevisiae* facilitates adaptation to a variety of stressful conditions like  
heat and pH<sup>70</sup>, copper<sup>8,17</sup>, salt<sup>11,46</sup>, and nutrient limitation<sup>12,19,1</sup>, with similar results in *Candida*  
54 *albicans*<sup>68</sup>. Importantly, aneuploidy can also lead to drug resistance in pathogenic fungi such as  
*C. albicans*<sup>54,53,16</sup> and *Cryptococcus neoformans*<sup>58</sup>, which cause candidiasis and meningoencephalitis,  
56 respectively. Although we focus here on aneuploidy, a similar phenomena of adaptation via gene  
duplication or amplification has been observed in yeast<sup>33</sup>, bacteria<sup>60</sup>, and DNA viruses<sup>13</sup>.  
58 Yona et al.<sup>70</sup> demonstrated experimentally the importance of aneuploidy in adaptive evolution. They  
evolved populations of *S. cerevisiae* under strong heat stress. The populations adapted to the heat stress  
60 within 450 generations, and this adaptation was determined to be due a duplication of Chromosome  
III. Later on, after more than 1,500 generations, the populations reverted back to an euploid state, while  
62 remaining adapted to the heat stress. Aneuploidy was therefore suggested to be a *transient adaptive*  
*solution*, because it can rapidly appear and fixate in the population under stressful conditions, and can  
64 then be rapidly lost when the cost of aneuploidy outweighs its benefit—after the stress is removed,  
or after "refined" beneficial mutations appear and fixate<sup>70</sup>. Furthermore, it has been suggested that

66 aneuploidy is an evolutionary "stepping stone" that facilitates future adaptation by genetic mutations,  
which require more time to evolve<sup>70,69</sup>.

68 Here, we test the hypothesis that aneuploidy is a an *evolutionary stepping stone* that facilitates  
adaptive evolution by genetic mutations Yona et al.<sup>69</sup>. We develop an evolutionary genetic model and  
70 fit it to the experimental results of Yona et al.<sup>70</sup> to predict the genotype frequency dynamics in the  
experimental populations, thereby estimating the frequency of evolved euploid cells that descended  
72 from aneuploid cells. Our results show that although aneuploidy reached high frequencies in the  
experimental populations, the majority of cells in the evolved euploid population likely did not  
74 descend from aneuploid cells, but rather directly from wild-type euploid cells. These suggests that at  
the lineage level, aneuploidy may be an evolutionary detour, rather than a stepping stone, on the path  
76 to adaptation.

## Results

78 In the heat-stress experiment of Yona et al.<sup>70</sup>, four populations of *S. cerevisiae* evolved under 39 °C.  
Aneuploidy fixed in all four experimental repetitions in the first 450 generations. Two of the repetitions,  
80 marked *H2* and *H4*, carried no large-scale duplications other than a Chromosome III trisomy. These  
two repetitions continued to evolve under the same conditions, wherein aneuploidy was eliminated by  
82 generation 1,700 and 2,350 in *H4* and *H2*, respectively.

**Evolutionary genetic model.** To explore the dynamics during the evolutionary experiments, we  
84 developed an evolutionary genetic model, fitted the model to empirical data, and used it to predict the  
genotype frequency dynamics, or specifically, the fraction of the evolved euploid population descended  
86 from aneuploid cells.

The model includes the effects of natural selection, genetic drift, aneuploidy, and mutation, and follows  
88 a population of cells characterized by their genotype: euploid wild-type,  $2n$ , is the ancestral diploid  
genotype; euploid mutant,  $2n^*$ , has a diploid karyotype and a single beneficial mutation; aneuploid  
90 wild-type,  $2n+1$ , has an extra chromosome due to a chromosome duplication event; and aneuploid  
mutant,  $2n+1^*$ , has and extra chromosome (like  $2n+1$ ) and a beneficial mutation (like  $2n^*$ ). Fitness  
92 values of the different genotypes are denoted by  $w_{2n}$ ,  $w_{2n^*}$ ,  $w_{2n+1}$ , and  $w_{2n+1^*}$ , and the rate of mutation  
and aneuploidy are denoted by  $\mu$  and  $\delta$ , respectively. See Figure 1 for an illustration of the model.

94 We fitted this model to the experimental results<sup>70</sup> – time for fixation (>95%) and for loss (<5%) of  
aneuploidy – using approximate Bayesian computation with sequential Monte Carlo (ABC-SMC)<sup>59</sup>,

96 thereby inferring the model parameters: rates aneuploidy and mutation and the fitness of all genotypes.  
 We then sampled posterior predictions for the genotype frequency dynamics using the estimated  
 98 parameter values and compared different versions of the model to test additional hypotheses about the evolutionary process.

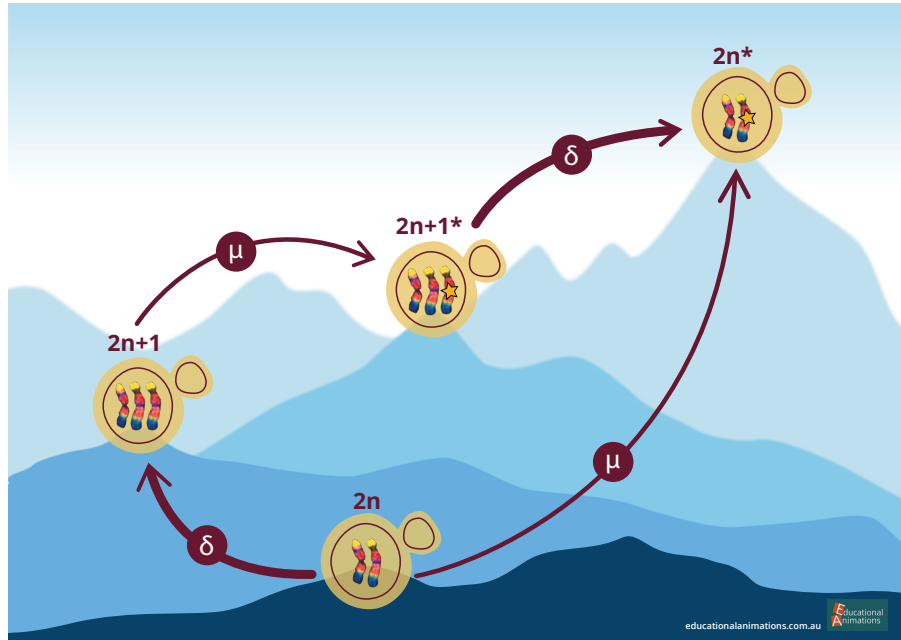


**Figure 1: Model Illustration.** There are four genotypes in our model: euploid wild-type,  $2n$ ; euploid mutant,  $2n^*$ ; aneuploid wild-type,  $2n+1$ ; and aneuploid mutant,  $2n+1^*$ . Overall there are two possible trajectories from  $2n$  to  $2n^*$ . Arrows denote transitions between genotypes, with transition rates  $\mu$  for the beneficial mutation rate and  $\delta$  for the aneuploidy rate. Elevation differences illustrate the expected, rather than the assumed, fitness differences between the genotypes.

100 **Estimated rates and fitness effects of aneuploidy and mutation.** We inferred the posterior distribution of model parameters (Figure 2). We report parameter estimates using the MAP (maximum a 102 posteriori) and providing the 50% HDI (highest density interval) in square brackets. See Supplementary Material for sensitivity analysis.

104 The estimated beneficial mutation rate is  $\mu = 2.965 \cdot 10^{-6}$  [ $2.718 \cdot 10^{-7} - 3.589 \cdot 10^{-6}$ ] per genome per generation. From the literature, the mutation rate per base pair is roughly  $2 - 3 \cdot 10^{-10}$  (refs. <sup>74,35</sup>), but 106 it may be higher under heat stress, as several stresses<sup>20</sup>, including heat<sup>22</sup>, may cause hypermutation in yeast. If we assume a 10-fold increase over the mutation rate reported in the literature, then the 108 estimated beneficial mutation rate can be explained by a genomic target size of 1,000 base pairs (that is, 1,000 base pairs across the genome in which a mutation would provide a fitness benefit). 110 Supporting this, Jarolim et al.<sup>25</sup> found 279 genes that contributed to survival after a sudden shift from 30 °C to 50 °C, and Flynn et al.<sup>14</sup> used a deep mutational scan of a single protein, Hsp90, to find 465

112 amino-acid variants that increased growth rate in 37 °C. Furthermore, Yona et al.<sup>70</sup> found at least 10  
114 genes on Chromosome III that increased heat tolerance when over-expressed. Assuming that other  
116 chromosomes also have a similar number of heat-tolerance genes (and even more, as Chromosome  
III is one of the smallest chromosomes<sup>18</sup>), we get a total of 160 heat-tolerance genes in the genome.  
Indeed, mutations were found in 97 genes in an evolutionary experiment with yeast under heat stress<sup>22</sup>.  
Thus, to get a genomic target size of 1,000, it is enough that the average gene target size (number of  
118 base pairs in a gene in which a mutation is beneficial) is 6.25 base pairs. For example, Kohn and  
Anderson<sup>30</sup> found a target size of 11 in a proton exporter gene (*PMA1*) that contributes to high-salt  
120 adaptation.

The estimated aneuploidy rate,  $\delta = 1.72 \cdot 10^{-3}$  [ $1.47 \cdot 10^{-3} - 2.786 \cdot 10^{-3}$ ] is higher than in previous  
122 studies: for Chromosome III in diploid *S. cerevisiae*, Zhu et al.<sup>74</sup> estimated  $6.7 \cdot 10^{-6}$  chromosome  
gain events per generation, and Kumaran et al.<sup>32</sup> estimate  $3.0 \cdot 10^{-5} - 4.3 \cdot 10^{-5}$  chromosome loss  
124 events per generation (95% confidence interval). However, this difference may be partly explained  
by an increased aneuploidy rate during heat stress: heat shock can increase the rate of chromosome  
126 fragment loss by 2-3 orders of magnitude<sup>5</sup>.

The estimated fitness values are  $w_{2n+1} = 1.022$  [1.021 – 1.023],  $w_{2n+1*} = 1.025$  [1.024 – 1.026],  
128  $w_{2n*} = 1.028$  [1.026 – 1.029], all relative to the fitness of  $2n$ , which is set to  $w_{2n} = 1$ . Thus, we  
can infer that the cost of Chromosome III trisomy is  $c = w_{2n*} - w_{2n+1*} = 0.003$  (or 0.3%) and the  
130 benefit of trisomy is  $w_{2n+1} - 1 - c = 0.019$  (1.9%), whereas the benefit of the beneficial mutation is  
 $w_{2n*} - 1 = 0.028$  (2.8%).

132 If we allow for transitions (mutation, chromosome loss and gain) to less-fit genotypes (e.g.,  $2n^*$  to  
 $2n+1^*$ ), then we infer similar but slightly different values, see Supplementary Material.

134 **Model comparison and goodness-of-fit.** To assess the fit of our model to the data, we use posterior  
predictive checks, in which we simulate the frequency dynamics using MAP parameter estimates and  
136 compare them to the data. Our model fits the data well:  $2n^*$  fixed in 63% of simulations by generation  
1,700 and in 100% of simulations by generation 2,350 (Figure 3).

138 However, a model without aneuploidy (where the aneuploidy rate is fixed at zero,  $\delta = 0$ ), fails to  
explain the experimental observations (Figure 3). The estimated mutation rate without aneuploidy is  
140  $\mu = 7.98 \cdot 10^{-9}$  [ $7.906 \cdot 10^{-9} - 8.138 \cdot 10^{-9}$ ], much lower compared to a model with aneuploidy. The  
fitness of the mutant is also much lower at  $w_{2n*} = 1.013$  [1.012 – 1.013]. This is because, without  
142 aneuploidy, a high mutation rate or fitness effect will lead to faster appearance and fixation of  $2n^*$  than

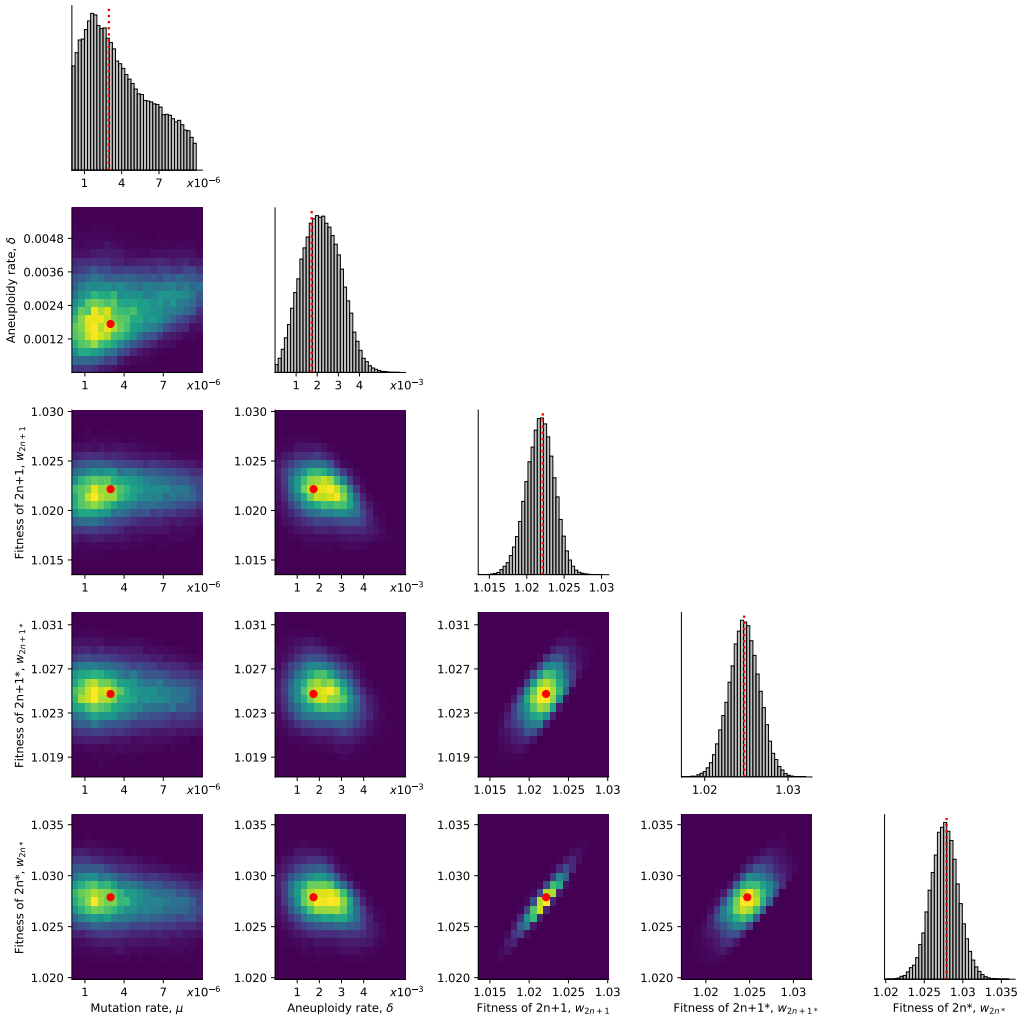


**Figure 2: Posterior distribution of model parameters.** On the diagonal, the marginal posterior distribution of each model parameter. Below the diagonal, the joint posterior distribution of pairs of model parameters (dark purple and bright yellow for low and high density, respectively). Red markers and orange lines for the joint MAP estimate (which may differ from the marginal MAP, as the marginal distribution integrates over all other parameters).

in the experimental observations.

- 144 We also checked a model in which aneuploidy occurs but is adaptively neutral compared to the wild-type, that is,  $w_{2n+1} = w_{2n}$  and  $w_{2n+1*} = w_{2n*}$  but  $\delta > 0$ . This model fits the data better than the model  
 146 with no aneuploidy (in which  $\delta = 0$ ), but worse than a model with positive selection for aneuploidy, in which  $w_{2n} < w_{2n+1} < w_{2n+1*} < w_{2n*}$  (Figure 3).

- 148 **Model predictions of genotype frequency dynamics.** We simulated 50 replicate genotype frequency dynamics using the MAP estimate parameters. Figure 4A shows the simulated frequencies of  
 150 the four genotypes ( $2n$ ,  $2n+1$ ,  $2n+1^*$  and  $2n^*$ ), as well as the frequencies of  $2n^*$  cells that arose from either  $2n+1$  cells via a sequences of mutation and chromosome loss events ( $2n_A^*$ ), or directly from

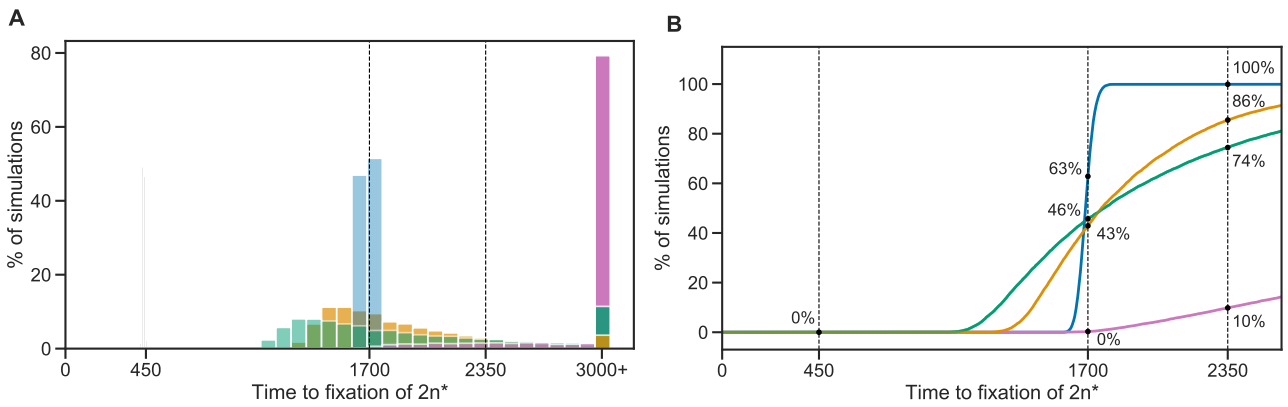


**Figure 3: Model fit with and without aneuploidy.** The distribution of time to fixation of  $2n^*$  (i.e., adaptation time) in 10,000 simulations using MAP parameters of the model with beneficial aneuploidy (blue;  $\delta > 0$ ,  $w_{2n} < w_{2n+1} < w_{2n+1}^* < w_{2n}^*$ ) compared to alternative models: a model with the same parameter values but without aneuploidy (gray,  $\delta = 0$ , concentrated at  $t = 450$ ); a model fitted to the data assuming no aneuploidy (green,  $\delta = 0$ ); a model fitted to the data assuming neutral aneuploidy (yellow,  $\delta > 0$ ,  $w_{2n+1} = w_{2n}$ ,  $w_{2n+1}^* = w_{2n}^*$ ); and a model with beneficial aneuploidy and an extended prior distribution (pink). In the experiment by Yona et al.<sup>70</sup>, one population lost aneuploidy by generation 1,700 and another by generation 2,350 (dashed lines) but not before generation 450. Thus, the blue distribution has a better fit compared to the other distributions (the gray distribution has a particularly poor fit). The MAP likelihood (eq. (4)) is 0.84, 0.78, 0.67, and 0.14 for the models represented by blue, yellow, green, and pink distributions, respectively. **(A)** Histogram of the time to fixation of  $2n^*$ . The last bin contains all values equal or greater than 3,000. **(B)** Cumulative distribution of the time to fixation.

- 152  $2n$  cells via a mutation event ( $2n_M^*$ ). We find that  $2n+1^*$  never reaches substantial frequency as it is quickly replaced by  $2n^*$  in a process similar to *stochastic tunneling*<sup>24,31</sup>.
- 154 To test the hypothesis that aneuploidy facilitates adaptation, we estimated  $F_A$ , the expected frequency of  $2n^*$  that arose from  $2n+1$ , computed as the average frequency of such  $2n_A^*$  cells at the end of
- 156 simulations using the MAP estimate parameters. Surprisingly, we observe that the majority of  $2n^*$  cells are  $2n_M^*$ , a product of a direct mutation in  $2n$  cells, rather than descending from  $2n+1$  cells
- 158 ( $F_A^{MAP} = 0.106$ , average end point of 50 purple lines in Figure 4A). This is despite the fact that the  $2n+1$  genotype reaches high frequencies in the population (at least 0.98, Figure 4A).
- 160 This result is not unique to the MAP parameter estimate. We simulated genotype frequency dynamics using parameter samples from the posterior distribution, and computed the posterior distribution of
- 162  $F_A$  (Figure 4B). The posterior mode  $F_A$  was just 0.147 [0.0154-0.370 95% CI] and only in 489 of 100,000 posterior samples (0.489%)  $F_A$  was larger than 0.5 (see Supporting Material for results when

164 transitions to less-fit genotypes are allowed, such as  $2n^*$  to  $2n+1^*$ ). Thus, if we sample a random  
165 cell from the evolved  $2n^*$  population, it is more likely to have descended directly from an euploid  
166 cell than from an aneuploid cell. The probability of  $2n^*$  descending from  $2n+1$  ( $F_A$ ) increases  
167 with the aneuploidy rate,  $\delta$ , and decreases with both the population size  $N$  and the mutation rate,  $\mu$   
168 (Figure 4C,D). In some cases it can also be affected by the fitness parameters (Figure S10).

**Genetic instability in aneuploid cells.** It has been suggested that aneuploidy increases genetic  
170 instability: Sheltzer et al.<sup>56</sup> have demonstrated a fold increase of between 2.2 and 7.1 in mutation  
171 rate. Therefore, we inferred model parameters under the assumption that the mutation rate increases  
172 in aneuploid cells by a factor  $\tau = 1, 33/32$  (due to an additional chromosome), 2, 5, 10, or 100 (due  
173 to genetic instability). We found that the posterior distribution was similar for  $\tau = 1, 33/32, 2$ , and 5  
174 (Figure S4). Furthermore, we computed the WAIC, a criterion for model selection (Methods). The  
175 WAIC values were similar for all  $\tau$  values (Table S1).

176 Assuming a strong increase of the mutation rate in aneuploid cells, i.e.  $\tau = 100$ , the inferred  
177 mutation rate was  $\mu = 4.094 \cdot 10^{-7}$  [ $6.252 \cdot 10^{-8} - 6.046 \cdot 10^{-7}$ ]), and the inferred aneuploidy rate  
178 that was  $\delta = 0.744 \cdot 10^{-3}$  [ $0.506 \cdot 10^{-3} - 1.827 \cdot 10^{-3}$ ]. Compared to inference made assuming no  
179 effect of aneuploidy on the mutation rate, these rates were about 7-8-fold and 2-3-fold lower for  $\mu$  and  
180  $\delta$ , respectively. Assuming  $\tau = 10$ , the inferred a mutation rate was only slightly lower compared to  
181  $\tau = 1$  ( $\mu = 1.67 \cdot 10^{-6}$  [ $2.836 \cdot 10^{-8} - 2.245 \cdot 10^{-6}$ ]).

182 Therefore, we do not find any evidence of an increase in mutation rate in aneuploid cells. This may  
183 be because, unless the increase is strong ( $\tau \geq 10$ ), it does not seem to affect our inference; or because  
184 Chromosome III is one of the smallest chromosomes<sup>18</sup>. We also checked the differences in genotype  
185 frequency dynamics for different  $\tau$  values. We observe  $\tau = 100$  could be distinguished if accurate  
186 data was available for the waiting time until the frequency of  $2n$  to decrease below 95% (Figure S5A)  
187 or for waiting time for the frequency of  $2n+1$  to either reach or go below 95% (Figure S5B). Similarly,  
188 we did not find evidence for an increase in the aneuploidy rate in aneuploid cells<sup>56</sup>, probably due to  
189 lack of statistical power.

## 190 Discussion

In a study on the role of chromosome duplication in adaptive evolution, Yona et al.<sup>70</sup> found that a  
192 Chromosome III trisomy was acquired by *S. cerevisiae* populations evolving under heat stress, only  
193 to be later replaced by euploid mutant cells that carry "refined" solutions to the stress. Additionally,  
194 such a replacement also occurred when they initiated evolutionary experiments with a population in

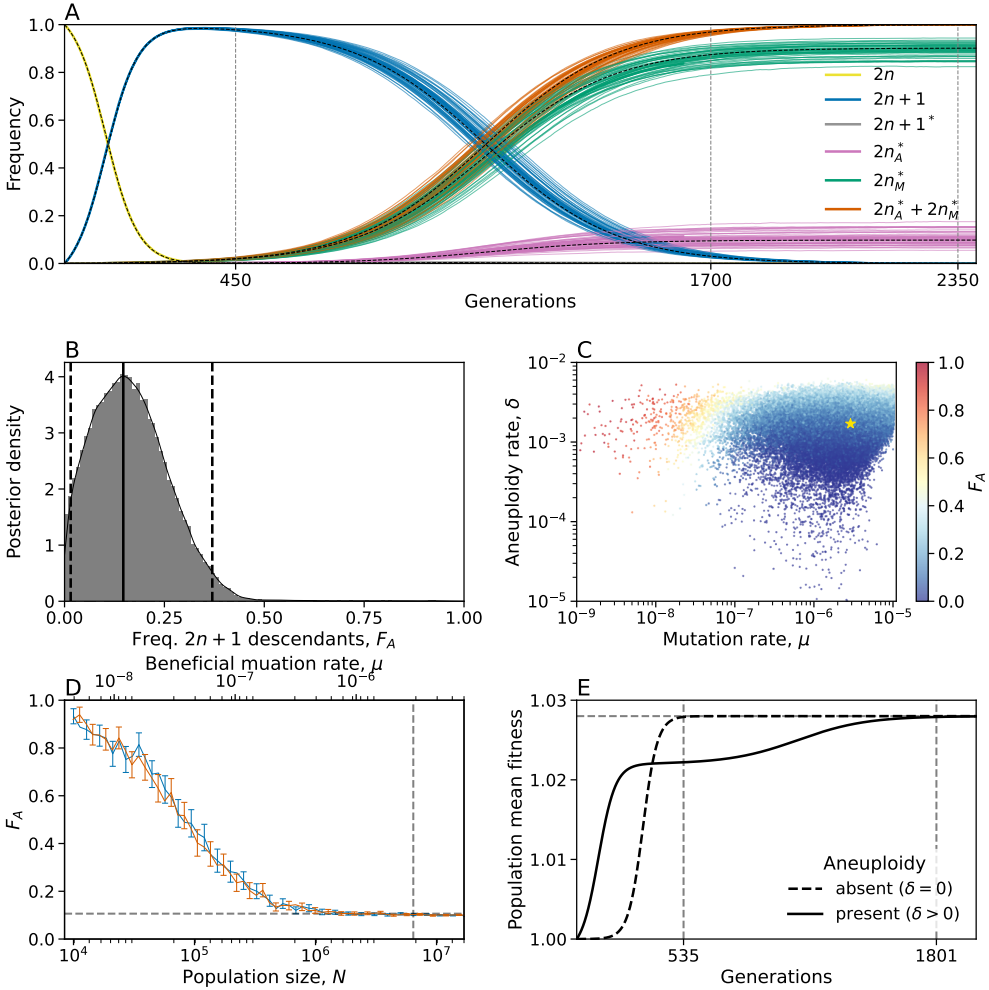


**Figure 4: Predicted frequency of aneuploid-descended cells.** (A) Posterior predicted genotype frequencies over time, including the source of  $2n^*$ :  $2n_A^*$  arose from  $2n+1$ , whereas  $2n_M^*$  arose directly from  $2n$ . Colored curves are 50 simulations using the MAP estimate parameters. Black dashed curves are the expected genotype frequencies without genetic drift (from a deterministic model). See Figure S9 for log-log scale, in which the sequence of events is easier to observe. (B) Posterior distribution of  $F_A$ , the expected frequency of  $2n^*$  cells descended from  $2n+1$  cells, computed as the average frequency at the end of 100 simulations for 100,000 samples from the parameter posterior distribution. Solid and dashed lines show the mode and 95% CI. (C)  $F_A$  values (color coded) from panel B, with their corresponding mutation rate  $\mu$  on x-axis and aneuploidy rate  $\delta$  on the y-axis. Yellow star shows the MAP estimate. See also Figure S10. (D)  $F_A$  as a function of the population size ( $N$ , bottom x-axis) and the beneficial mutation rate ( $\mu$ , top x-axis) in posterior predictions with MAP parameters. Markers show  $F_A$  in 250 simulations per population size or mutation rate value. Error bars show mean  $F_A$  with 95% CI (bootstrap,  $n = 10,000$ ). Blue and red bars for varying population size and mutation rate, respectively. Vertical dashed line for population size in the experiment,  $6.425 \cdot 10^6$ , and the MAP mutation rate,  $2.965 \cdot 10^{-6}$ . Horizontal line for  $F_A^{MAP} = 0.106$ . (E) Population mean fitness in a model without drift using MAP estimate parameters. Solid lines for mean fitness with aneuploidy ( $\delta > 0$ ), where the population reaches adaptation (mean fitness at 99.99% of maximum value) at generation 1,802. Dashed lines for mean fitness without aneuploidy ( $\delta = 0$ ), where the population adapts much earlier, at generation 535.

which all cells carry a Chromosome III trisomy. They hypothesized that aneuploidy is a “useful yet  
196 short-lived intermediate that facilitates further adaptation”, suggesting that the euploid mutant cells  
evolved by heat-resistance mutations in aneuploid cells followed by reversion of trisomy due to a  
198 chromosome loss event.

We developed an evolutionary genetic model of adaptive evolution by aneuploidy and mutation  
200 (Figure 1), fitted it to the experimental results of Yona et al.<sup>70</sup>, and used it to predict the genotype  
frequency dynamics. The model predicted that only about 10-15% of the evolved euploid population  
202 descended from aneuploid cells by acquiring a mutation and losing the extra chromosome—that is,  
the majority of the euploid population are not descended from aneuploid cells, but rather are direct  
204 descendants of the ancestral wild-type population (Figure 4).

This happens despite aneuploidy reaching a high frequency in the population (>95%). Conventional  
206 wisdom might suggest that once the aneuploid genotype  $2n+1$  reaches high frequency, it will have a  
better chance at producing "refined" solutions via mutations, and its descendants will come to dominate  
208 the population: the frequency of  $2n_A^*$  (which arises from  $2n+1^*$ ) will be higher than the frequency of  
 $2n_M^*$  (which arises directly from  $2n$ ).

210 So how does  $2n_M^*$  prevail? Initially, the supply rates of  $2n+1$  and  $2n_M^*$  are  $N\delta \approx 11,000$  and  $N\mu \approx 19$ ,  
respectively (assuming MAP parameter estimates). Therefore, both genotypes are expected to appear  
212 immediately at the beginning of the experiment (Figure S9). However,  $2n+1$  appears at a much higher  
frequency as  $\delta \gg \mu$  by 2-3 orders of magnitude. After they first appear,  $2n_M^*$  has higher fitness. But  
214 as long as the frequency of  $2n$  is high, the supply rate of  $2n+1$  is higher than that of  $2n_M^*$ , again due to  
 $\delta \gg \mu$ . However, supply rates of both genotypes decreases with the frequency of  $2n$ . Therefore, when  
216 the latter decreases, mainly due to the increase in the frequency of  $2n+1$ , both supply rates diminish.  
At this stage, the higher fitness of  $2n_M^*$  comes into play and it starts to take over the population, which  
218 is mainly composed of  $2n+1$ . For the aneuploid lineage to compete with the mutant lineage, it must  
produce  $2n_A^*$  via a mutation followed by chromosome loss. Although this is a stochastic process  
220 (due to drift), our results show that the time until  $2n_A^*$  reaches a frequency of 0.1% is roughly 450  
generations, without much variation (intersection of purple lines and vertical dashed line in Figure S9).  
222 However, by that time  $2n_M^*$  is already at a roughly 10-fold higher frequency (1.86%), and since both  
mutants have the same fitness, their relative frequency remains roughly the same until the end of the  
224 experiment.

**Predictions for small populations and low mutation rates.** We examined the effect of the popula-  
226 tion size,  $N$ , and the beneficial mutation rate,  $\mu$ , on the frequency of  $2n+1$  descendants in the evolved

population,  $F_A$ . We found that  $F_A$  is expected to decrease as the population size or mutation rate increase (Figure 4D), ranging from  $>90\%$  when the population size is 10,000 or the mutation rate is  $6 \cdot 10^{-9}$ , to about 10% when the population size is above 1,000,000 (less than the experimental population size, which was 6,425,000) or the mutation rate is above  $2 \cdot 10^{-6}$  (less than the inferred mutation rate, which is  $2.965 \cdot 10^{-6}$ ). Thus, our model provides a testable prediction: if the experiment was repeated under a lower population size (via stronger daily dilutions or in a smaller volume) or a lower mutation rate (via a non-mutagenic stress or stress with a smaller target size such as drug resistance), then the fraction of the population descending from aneuploid cells would be much higher.

**Aneuploidy delays rather than facilitates adaptation.** An additional interesting result of our study is that aneuploidy increases, rather than decreases, the adaptation time (Figure 4E). This happens despite the fact that the mean fitness initially increases faster in the presence of aneuploidy (Figure 4E). This is because once  $2n+1$  is common, selection for the mutant strain ( $2n+1^*$  or  $2n^*$ ) is weaker compared to when  $2n^*$  competes directly with  $2n$ .

**Rate and fitness effect of aneuploidy and mutation.** We inferred the rates of aneuploidy and mutation and their effects on fitness. We estimate that the aneuploidy rate (i.e., number of chromosome gains per generation) is  $1.7 \cdot 10^{-3}$ , higher than a previous estimate of  $6.7 \cdot 10^{-6}$  (ref<sup>73</sup>). This may be due to genetic instability caused by heat stress<sup>5</sup>. In addition, we find no evidence for increased mutation rates in aneuploid cells. Previous empirical studies have suggested that genetic instability (e.g., elevated mutation rates) in aneuploid cells is due to stress associated with the aneuploid state<sup>3,6,71,23</sup>. However, in the experiment of Yona et al.<sup>70</sup>, both the wild-type and the aneuploid were under heat stress, which may explain why we did not find evidence for an increased mutation rate specifically in aneuploid cells.

**Conclusions.** Here, we tested the hypothesis that aneuploidy cells are an evolutionary "stepping stone", or adaptive intermediate, between wild-type euploid cells and mutant euploid cells<sup>69</sup>. Our results suggest that, although it seems the population goes from euploid to aneuploid and back, this is not the case at the individual level. We estimate that only about 10-15% of the euploid cells descended from aneuploid cells, whereas the rest are direct descendants of the wild-type euploid cells. Thus, aneuploidy can delay, rather than accelerate, adaptation, and cells that become aneuploid may leave less descendants than cells that remain euploid. This surprising result reinforces the importance of mathematical models when interpreting evolutionary dynamics. Moreover, our study emphasizes the unintuitive outcomes of clonal interference between mechanisms for generation of variation that differ

258 in their rate of formation and distribution of fitness effects, including mutation, copy number variation, horizontal gene transfer, and epigenetic modifications.

## 260 Models and Methods

**Evolutionary genetic model.** We model the evolution of a population of cells using a Wright-Fisher model<sup>40</sup>, assuming a constant effective population size  $N$ , non-overlapping generations, and including the effects of natural selection, genetic drift, aneuploidy, and mutation. We focus on beneficial genetic modifications, neglecting the effects of deleterious and neutral mutations or karyotypic changes. The model allows for a single aneuploid karyotype (e.g., Chromosome III duplication) and a single mutation to accumulate in the genotype. Thus, the model follows four genotypes (Figure 1): euploid wild-type,  $2n$ , the initial genotype; euploid mutant,  $2n^*$ , with the standard karyotype and a single beneficial mutation; aneuploid wild-type,  $2n+1$ , with an extra chromosome, i.e., following chromosome duplication; and aneuploid mutant,  $2n+1^*$ , with an extra chromosome and a beneficial mutation.

Transitions between the genotypes occur as follows (Figure 1): Beneficial mutations from  $2n$  to  $2n^*$  and from  $2n+1$  to  $2n+1^*$  occur with probability  $\mu$ , the mutation rate. We neglect back-mutations (i.e., from  $2n^*$  to  $2n$  and from  $2n+1^*$  to  $2n+1$ ). Aneuploidy is formed by chromosome mis-segregation, so that cells transition from  $2n$  to  $2n+1$  and from  $2n+1^*$  to  $2n^*$  with probability  $\delta$ , the aneuploidy rate. That is, we assume chromosomes are gained and lost at the same rate, and we neglect events that form a less-fit genotype (i.e.,  $2n+1$  to  $2n$  and  $2n^*$  to  $2n+1^*$ ). A model that assumed increased aneuploidy rates in aneuploid cells (as in Sheltzer et al.<sup>56</sup>) did not perform well, probably due to lack of statistical power, and was abandoned.

In the experiment by Yona et al.<sup>70</sup>, the population was grown every day from  $1.6 \cdot 10^6$  cells until reaching stationary phase and then diluted 1:120. Thus, we set the population size to  $N = 6.425 \cdot 10^6$ , the harmonic mean of  $\{2^k \cdot 1.6 \cdot 10^6\}_{k=0}^7$ <sup>10</sup>. The initial population has  $N$  cells with genotype  $2n$ . The effect of natural selection on the frequency  $f_i$  of genotype  $i = 2n, 2n+1, 2n+1^*$ , or  $2n^*$  is given by

$$284 \quad f_i^s = \frac{f_i w_i}{\bar{w}} , \quad (1)$$

where  $w_i$  is the fitness of genotype  $i$  and  $\bar{w} = \sum_j f_j w_j$  is the population mean fitness. The effect of

286 mutation and aneuploidy on genotype frequencies is given by

$$\begin{aligned} f_{2n}^m &= (1 - \delta - \mu) f_{2n}^s, \\ f_{2n+1}^m &= \delta f_{2n}^s + (1 - \mu) f_{2n+1}^s, \\ f_{2n+1^*}^m &= \mu f_{2n+1}^s + (1 - \delta) f_{2n+1^*}^s, \\ f_{2n^*}^m &= \mu f_{2n}^s + \delta f_{2n+1}^s + f_{2n^*}^s. \end{aligned} \tag{2}$$

288 Finally, random genetic drift is modeled using a multinomial distribution<sup>40</sup>,

$$\mathbf{f}' \sim \frac{1}{N} \cdot \text{Mult}(N, \mathbf{f}^m), \tag{3}$$

290 where  $\mathbf{f}^m = (f_{2n}^m, f_{2n+1}^m, f_{2n+1^*}^m, f_{2n^*}^m)$  are the frequencies of the genotypes after mutation and  
 292 aneuploidy,  $\mathbf{f}'$  are the genotype frequencies in the next generation, and  $\text{Mult}(N, \mathbf{f})$  is a multinomial  
 distribution parameterized by the population size  $N$  and the genotype frequencies  $\mathbf{f}$ . Overall, the change  
 in genotype frequencies from one generation to the next is given by the transformation  $f_i \rightarrow f'_i$ .

294 **Empirical data for model inference.** We use the results of evolutionary experiments reported by  
 Yona et al.<sup>70</sup>. In their heat-stress experiment, four populations of *S. cerevisiae* evolved under 39 °C.  
 296 Aneuploidy fixed in all four population in the first 450 generations. Hereafter, fixation or elimination  
 of a genotype by *generation t* means that more than 95% or less than 5% of the population carry the  
 298 genotype at generation  $t$ , and possibly earlier. From re-analysis of data not published in the original  
 paper, aneuploidy did not fix before at least 200 generations elapsed. The experiment continued with  
 300 two populations, in which aneuploidy was eliminated by generation 1,700 and 2,350 while still under  
 the same conditions of elevated heat (39 °C).

302 **Likelihood function.** Because our model, just like the Wright-Fisher model, is non-linear and  
 stochastic, computing the distribution of fixation time  $T(g)$  of genotype  $g$  for use in the likelihood  
 304 function is intractable (it is even hard to use a diffusion-equation approximation due to the model having  
 multiple genotypes, rather than just two). We overcome this problem by approximating the likelihood  
 306 using simulations. We simulate 1,000 experiments per parameter vector  $\theta = (\mu, \delta, s, b, c)$ , resulting  
 in a set of simulated observations  $\tilde{\mathbf{X}} = \{\tilde{X}_i\}_{i=1}^{1000}$ . We then compute the approximate likelihood,

$$\begin{aligned} \mathcal{L}(\theta) &= P^4(200 \leq T(2n+1) \leq 450) \cdot \left[ 1 - \right. \\ &\quad P_{\tilde{\mathbf{X}}}^4(\{T(2n^*) < 1700\} \mid 200 \leq T(2n+1) \leq 450) - \\ &\quad P_{\tilde{\mathbf{X}}}^4(\{1700 < T(2n^*) < 2350\} \mid 200 \leq T(2n+1) \leq 450) + \\ &\quad \left. P_{\tilde{\mathbf{X}}}^4(\{T(2n^*) < 1700\} \wedge \{1700 < T(2n^*) < 2350\} \mid 200 \leq T(2n+1) \leq 450) \right], \end{aligned} \tag{4}$$

308

where  $!\{\dots\}$  is the "logical not" operator,  $P^4(\dots)$  is the 4th power of  $P(\dots)$ , and all probabilities  $P_{\tilde{\mathbf{X}}}(\dots)$  are approximated from the results of the simulations  $\tilde{\mathbf{X}}$ . For example,  $P_{\tilde{\mathbf{X}}}(!\{T(2n^*) < 1700\} \mid 200 \leq T(2n+1) \leq 450)$  is approximated by taking simulations in which  $2n+1$  fixed before generation 450 but not before generation 200, and computing the fraction of such simulations in which  $2n^*$  did not fix by generation 1,700, and hence aneuploidy did not extinct before generation 1,700. Figure S1 compares results with less and more simulated experiments, demonstrating that 1,000 simulations are likely sufficient.

For a model without aneuploidy (that is, when the aneuploidy rate is fixed at zero,  $\delta = 0$ ), we disregard the increased expression in Chromosome III and the growth advantage measured in generation 450, and focus on the growth advantage measured in later generations, presumably due to a beneficial mutation. Therefore, the likelihood is approximated by

$$\begin{aligned} \mathcal{L}_!(\theta) = 1 - P_{\tilde{\mathbf{X}}}^4(!\{T(2n^*) < 1700\}) - \\ P_{\tilde{\mathbf{X}}}^4(!\{1700 < T(2n^*) < 2350\}) + \\ P_{\tilde{\mathbf{X}}}^4(!\{T(2n^*) < 1700\} \wedge !\{1700 < T(2n^*) < 2350\}). \end{aligned} \quad (5)$$

**Parameter inference.** To infer model parameters, we use approximate Bayesian computation with a sequential Monte-Carlo scheme, or ABC-SMC<sup>59</sup>, implemented in the pyABC Python package<sup>29</sup> [pyabc.readthedocs.io](https://pyabc.readthedocs.io). This approach uses numerical stochastic simulations of the model to infer a posterior distribution over the model parameters. It is a method of likelihood-free, simulation-based inference<sup>9</sup>, that is, for estimating a posterior distribution when a likelihood function cannot be directly computed. It is therefore suitable in our case, in which the likelihood function can only be approximated from simulations, and cannot be directly computed.

The ABC-SMC algorithm employs sequential importance sampling over multiple iterations<sup>63,28,61</sup>. In iteration  $t$  of the algorithm, a set of parameter vectors,  $\{\theta_{i,t}\}_{i=1}^{n_t}$ , also called *particles*, are constructed in the following way. A proposal particle,  $\theta^*$ , is sampled from a proposal distribution, and is either accepted or rejected, until  $n_t$  particles are accepted. The number of particles,  $n_t$ , is adapted at every iteration  $t$  using the adaptive population strategy<sup>29</sup> [pyabc.readthedocs.io](https://pyabc.readthedocs.io). For  $t = 0$ , the proposal particle is sampled from the prior distribution,  $p(\theta)$ . For  $t > 0$ , the proposal particle is sampled from the particles accepted in the previous iteration,  $\{\theta_{i,t-1}\}_{i=1}^{n_{t-1}}$ , each with a probability relative to its weight  $W_{t-1}(\theta_{i,t-1})$  (see below). The proposal particle is then perturbed using a kernel perturbation kernel,  $K_t(\theta^* \mid \theta)$  where  $\theta$  is the sample from the previous iteration. Then, a set of synthetic observations  $\tilde{\mathbf{X}}^*$  is simulated, and the proposal particle  $\theta^*$  is accepted if its approximate likelihood (eq. (4)) is high enough,  $\mathcal{L}(\theta^*) > 1 - \epsilon_t$  (or more commonly, if  $1 - \mathcal{L}(\theta^*) < \epsilon_t$ ), where  $\epsilon_t > 0$  is the *acceptance*

*threshold*, as higher values of  $\epsilon_t$  allow more particles to be accepted. The acceptance threshold  $\epsilon_t$  is chosen as the median of the  $1 - \mathcal{L}(\theta)$  of the particles accepted in the previous iteration,  $t - 1$ , and  $\epsilon_0 = 0.01$ . For each accepted particle  $\theta_{i,t}$  a weight  $W_t(\theta_{i,t})$  is assigned: for  $t = 0$ ,  $W_0(\theta_{i,0}) = 1$ , and for  $t > 0$ ,  $W_t(\theta_{i,t}) = p(\theta_{i,t}) / \sum_{i=1}^{n_{t-1}} W_{t-1}(\theta_{i,t-1}) K_t(\theta_{i,t}, \theta_{i,t-1})$ , where  $p(\theta)$  is the prior density of  $\theta$  and  $K_t(\theta', \theta)$  is the probability of a perturbation from  $\theta$  to  $\theta'$ .  $K_t(\theta' | \theta)$  is a multivariate normal distribution, fitted at iteration  $t$  to the particles from the previous iteration,  $\{\theta_{i,t-1}\}_{i=1}^{n_{t-1}}$ , and their weights,  $\{W(\theta_{i,t-1})\}_{i=1}^{n_{t-1}}$ .

Acceptance is determined according to the approximate likelihood (eq. (4)), which has a maximum value of  $\mathcal{L}_{max} = 0.875$  (giving a minimal value of  $\epsilon_{min} = 0.125$ ). We terminated the inference iterations when the change in  $\epsilon$  value from one iteration to the next was small. With our standard prior and model, we reached  $\epsilon = 0.13$  (or  $\mathcal{L} = 0.87$ ) after six iterations, with  $n_6 = 982$  accepted parameter vectors and effective sample size ESS=651 (Figure S2). Running the inference algorithm with different initialization seeds and less or more simulations for approximating the likelihood produced similar posterior distributions (Figure S1).

After producing a set of weighted particles from the the posterior distribution using the above ABC-SMC algorithm, we approximate the posterior using kernel density estimation (KDE) with Gaussian kernels. We truncate the estimated posterior to avoid positive posterior density for values with zero prior density. The MAP (maximum a posteriori) estimate is computed as the the maximum of the estimated joint posterior density. We then draw 5,000,000 samples from the posterior distribution to compute the HDI (highest density interval) and draw 50,000 samples to visualize the posterior distribution with histograms.

**Model comparison.** We examine several versions of our evolutionary models, e.g. without aneuploidy or with increased mutation rate in aneuploid cells, as well as several different prior distributions (see below). To compare these, we plot posterior predictions: for each model we execute 10,000 simulations using the MAP parameter estimates and plot the distributions of time to fixation of  $2n^*$ , one of key properties of the model likelihood. These plots visualize the fit of each model to the data. Also, for similar models we plot the marginal and joint posterior distributions of the parameters; if these are similar, we consider the models interchangeable. We validate this by comparing HDI (highest density interval) of posterior distributions.

Where posterior plots are very similar and the number of parameters is the same, we use WAIC, or

the widely applicable information criterion<sup>15</sup>, defined as

370  $WAIC(\theta) = -2 \log \mathbb{E}[\mathcal{L}(\theta)] + 2\mathbb{V}[\log \mathcal{L}(\theta)]$  (6)

where  $\theta$  is a parameter vector, and  $\mathbb{E}[\cdot]$  and  $\mathbb{V}[\cdot]$  are the expectation and variance taken over the posterior distribution, which in practice are approximated using 50,000 samples from the posterior KDE. We validated that upon resampling WAIC values do not significantly change and that differences in WAIC between models are preserved. WAIC values are scaled as a deviance measure: lower values imply higher predictive accuracy.

376 **Prior distributions.** We used informative prior distributions for  $w_{2n+1} = 1 - c + b$ ,  $w_{2n+1*} = (1 + s)(1 - c) + b$  and  $w_{2n*} = 1 + s$ , which we estimated from growth curves data from mono-culture growth experiments previously reported by Yona et al.<sup>70</sup>, Figs. 3C, 4A, and S2. We used Curveball, a method for predicting results of competition experiments from growth curve data<sup>43</sup> [curveball.yoavram.com](http://curveball.yoavram.com). Briefly, Curveball takes growth curves of two strains growing separately in mono-culture and predicts how they would grow in a mixed culture, that is, it predicts the results of a competition assay. From these predictions, relative fitness values can be computed. Because Curveball uses a maximum-likelihood approach to estimate model parameters, we were able to estimate a distribution of relative fitness values to be used as a prior distribution by sampling 10,000 samples from a truncated multivariate normal distribution defined by the maximum-likelihood covariance matrix (Figure S3).

386 We used growth curves of  $2n$  and  $2n+1$  in 39 °C to estimate an informative prior distribution for  $w_{2n+1}$  (Figure S3D, assuming  $w_{2n} = 1$ ). In this prior distribution, we used the same prior for  $w_{2n+1*}$  and  $w_{2n*}$ . To increase computational efficiency, we also assumed  $w_{2n*} > w_{2n+1*} > w_{2n+1} > w_{2n}$ ; running the inference without this assumption produced similar results. See *supporting material* for 390 an extended informative prior distribution that uses growth curves of  $2n*$  and  $2n+1$  growing in 39 °C; this prior distribution proved to be less useful.

392 As a control, we tested an uninformative uniform prior with  $U(1, 6)$ , for (i) all  $w_{2n+1}$ ,  $w_{2n+1*}$ ,  $w_{2n*}$ , or (ii) only for  $w_{2n+1*}$ ,  $w_{2n*}$ , using the above informative prior for  $w_{2n+1}$ . In these cases the inference 394 algorithm failed to converge.

For the mutation rate,  $\mu$ , and aneuploidy rate,  $\delta$ , we used uninformative uniform priors,  $\mu \sim 396 U(10^{-9}, 10^{-5})$  and  $\delta \sim U(10^{-6}, 10^{-2})$ . A wider mutation rate prior,  $\mu \sim U(10^{-9}, 10^{-3})$ , produced similar results.

## 398 Acknowledgements

We thank Lilach Hadany, Judith Berman, David Gresham, Shay Covo, Martin Kupiec, Uri Obolski, Daniel  
400 Weissman, and Tal Simon for discussions and comments. This work was supported in part by the Israel  
Science Foundation (ISF, YR 552/19), the US–Israel Binational Science Foundation (BSF, YR 2021276),  
402 Minerva Center for Live Emulation of Evolution in the Lab (YR, YP), Minerva Stiftung short-term research  
grant (MP).

## 404 References

- [1] Avecilla, G., Chuong, J. N., Li, F., Sherlock, G., Gresham, D. and Ram, Y. 2022, ‘Neural networks enable efficient and accurate simulation-based inference of evolutionary parameters from adaptation dynamics’, *PLOS Biology* **20**(5), e3001633.
- [2] Bakhoum, S. F. and Landau, D. A. 2017, ‘Chromosomal instability as a driver of tumor heterogeneity and evolution’, *Cold Spring Harb. Perspect. Med.* **7**(6), 1–14.
- [3] Bouchonville, K., Forche, A., Tang, K. E. S., Semple, C. a. M. and Berman, J. 2009, ‘Aneuploid chromosomes are highly unstable during dna transformation of *Candida albicans*.’, *Eukaryot. Cell* **8**(10), 1554–66.
- [4] Boveri, T. 2008, ‘Concerning the origin of malignant tumours’, *J. Cell Sci.* **121**(Supplement 1), 1–84.
- [5] Chen, G., Bradford, W. D., Seidel, C. W. and Li, R. 2012, ‘Hsp90 stress potentiates rapid cellular adaptation through induction of aneuploidy.’, *Nature* **482**(7384), 246–50.
- [6] Chen, G., Rubinstein, B. and Li, R. 2012, ‘Whole chromosome aneuploidy: Big mutations drive adaptation by phenotypic leap’, *BioEssays* **34**(10), 893–900.
- [7] Cherry, J. M., Hong, E. L., Amundsen, C., Balakrishnan, R., Binkley, G., Chan, E. T., Christie, K. R., Costanzo, M. C., Dwight, S. S., Engel, S. R. et al. 2012, ‘Saccharomyces genome database: the genomics resource of budding yeast’, *Nucleic acids research* **40**(D1), D700–D705.
- [8] Covo, S., Puccia, C. M., Argueso, J. L., Gordenin, D. A. and Resnick, M. A. 2014, ‘The sister chromatid cohesion pathway suppresses multiple chromosome gain and chromosome amplification.’, *Genetics* **196**(2), 373–384.
- [9] Cranmer, K., Brehmer, J. and Louppe, G. 2020, ‘The frontier of simulation-based inference’, *Proceedings of the National Academy of Sciences* p. 201912789.

- [10] Crow, J. F. and Kimura, M. 1970, *An introduction to population genetics theory*, Burgess Pub. Co., Minneapolis.
- [11] Dhar, R., Sägesser, R., Weikert, C., Yuan, J. and Wagner, A. 2011, ‘Adaptation of *Saccharomyces cerevisiae* to saline stress through laboratory evolution.’, *J. Evol. Biol.* **24**(5), 1135–53.
- [12] Dunham, M. J., Badrane, H., Ferea, T., Adams, J., Brown, P. O., Rosenzweig, F. and Botstein, D. 2002, ‘Characteristic genome rearrangements in experimental evolution of *Saccharomyces cerevisiae*’, *Proc. Natl. Acad. Sci.* **99**(25), 16144–16149.
- [13] Elde, Nels, C., Child, Stephanie, J., Eickbush, Michael, T., Kitzman, Jacob, O., Rogers, Kelsey, S., Shendure, J., Geballe, Adam, P. and Malik, Harmit, S. 2012, ‘Poxviruses deploy genomic accordions to adapt rapidly against host antiviral defenses’, *Cell* **150**(4), 831–841.
- [14] Flynn, J. M., Rossouw, A., Cote-Hammarlof, P., Fragata, I., Mavor, D., Hollins, C., Bank, C. and Bolon, D. N. 2020, ‘Comprehensive fitness maps of hsp90 show widespread environmental dependence’, *Elife* **9**, 1–25.
- [15] Gelman, A., Carlin, J. B., Stern, H. S., Dunson, D. B., Vehtari, A. and Rubin, D. B. 2013, *Bayesian Data Analysis, Third Edition*, Chapman & Hall/CRC Texts in Statistical Science, Taylor & Francis.
- [16] Gerstein, A. C. and Berman, J. 2020, ‘*Candida albicans* genetic background influences mean and heterogeneity of drug responses and genome stability during evolution in fluconazole’, *mSphere* **5**(3).
- [17] Gerstein, A. C., Ono, J., Lo, D. S., Campbell, M. L., Kuzmin, A. and Otto, S. P. 2015, ‘Too much of a good thing: the unique and repeated paths toward copper adaptation.’, *Genetics* **199**(2), 555–71.
- [18] Gilchrist, C. and Stelkens, R. 2019, ‘Aneuploidy in yeast: Segregation error or adaptation mechanism?’, *Yeast* **36**(9), 525–539.
- [19] Gresham, D., Desai, M. M., Tucker, C. M., Jenq, H. T., Pai, D. A., Ward, A., DeSevo, C. G., Botstein, D. and Dunham, M. J. 2008, ‘The repertoire and dynamics of evolutionary adaptations to controlled nutrient-limited environments in yeast’, *PLoS Genet.* **4**(12).
- [20] Heidenreich, E. 2007, ‘Adaptive Mutation in *Saccharomyces cerevisiae*’, *Crit. Rev. Biochem. Mol. Biol.* **42**(4), 285–311.

- 456 [21] Hong, J. and Gresham, D. 2014, ‘Molecular specificity, convergence and constraint shape adaptive evolution in nutrient-poor environments’, *PLoS Genet.* **10**(1).
- 458 [22] Huang, C. J., Lu, M. Y., Chang, Y. W. and Li, W. H. 2018, ‘Experimental Evolution of Yeast for High-Temperature Tolerance’, *Mol. Biol. Evol.* **35**(8), 1823–1839.
- 460 [23] Ippolito, M. R., Martis, V., Martin, S., Tijhuis, A. E., Hong, C., Wardenaar, R., Dumont, M., Zerbib, J., Spierings, D. C., Fachinetti, D., Ben-David, U., Fojer, F. and Santaguida, S.
- 462 2021, ‘Gene copy-number changes and chromosomal instability induced by aneuploidy confer resistance to chemotherapy’, *Dev. Cell* **56**(17), 2440–2454.e6.
- 464 [24] Iwasa, Y., Michor, F. and Nowak, M. A. 2004, ‘Stochastic tunnels in evolutionary dynamics’, *Genetics* **166**(3), 1571–1579.
- 466 [25] Jarolim, S., Ayer, A., Pillay, B., Gee, A. C., Phrakaysone, A., Perrone, G. G., Breitenbach, M. and Dawes, I. W. 2013, ‘Saccharomyces cerevisiae genes involved in survival of heat shock’, *G3 Genes, Genomes, Genetics* **3**(12), 2321–2333.
- [26] Kass, R. E. and Raftery, A. E. 1995, ‘Bayes factors’, *J. Am. Stat. Assoc.* **90**(430), 773.
- 470 [27] Kasuga, T., Bui, M., Bernhardt, E., Swiecki, T., Aram, K., Cano, L. M., Webber, J., Brasier, C., Press, C., Grünwald, N. J., Rizzo, D. M. and Garbelotto, M. 2016, ‘Host-induced aneuploidy and phenotypic diversification in the sudden oak death pathogen *Phytophthora ramorum*’, *BMC Genomics* **17**(1), 1–17.
- 474 [28] Klinger, E. and Hasenauer, J. 2017, A scheme for adaptive selection of population sizes in approximate bayesian computation - sequential monte carlo, in J. Feret and H. Koepll, eds, ‘Computational Methods in Systems Biology’, Vol. 10545, Springer International Publishing, pp. 128–144. Series Title: Lecture Notes in Computer Science.
- 476 [29] Klinger, E., Rickert, D. and Hasenauer, J. 2018, ‘pyabc: distributed, likelihood-free inference’, *Bioinformatics* (May), 1–3.
- 480 [30] Kohn, L. M. and Anderson, J. B. 2014, ‘The underlying structure of adaptation under strong selection in 12 experimental yeast populations’, *Eukaryot. Cell* **13**(9), 1200–1206.
- 482 [31] Komarova, N. L., Sengupta, A. and Nowak, M. A. 2003, ‘Mutation-selection networks of cancer initiation: Tumor suppressor genes and chromosomal instability’, *Journal of Theoretical Biology* **223**(4), 433–450.

- [32] Kumaran, R., Yang, S.-Y. and Leu, J.-Y. 2013, ‘Characterization of chromosome stability in diploid, polyploid and hybrid yeast cells’, *PLoS ONE* **8**(7), e68094.
- [33] Lauer, S., Avecilla, G., Spealman, P., Sethia, G., Brandt, N., Levy, S. F. and Gresham, D. 2018, ‘Single-cell copy number variant detection reveals the dynamics and diversity of adaptation.’, *PLOS Biology* **16**.
- [34] Lukow, D. A., Sausville, E. L., Suri, P., Chunduri, N. K., Wieland, A., Leu, J., Smith, J. C., Girish, V., Kumar, A. A., Kendall, J., Wang, Z., Storchova, Z. and Sheltzer, J. M. 2021, ‘Chromosomal instability accelerates the evolution of resistance to anti-cancer therapies’, *Developmental Cell* **56**(17), 2427–2439.e4.
- [35] Lynch, M., Sung, W., Morris, K., Coffey, N., Landry, C. R., Dopman, E. B., Dickinson, W. J., Okamoto, K., Kulkarni, S., Hartl, D. L. and Thomas, W. K. 2008, ‘A genome-wide view of the spectrum of spontaneous mutations in yeast’, *Proceedings of the National Academy of Sciences* **105**(27), 9272–9277.
- [36] Mannaert, A., Downing, T., Imamura, H. and Dujardin, J. C. 2012, ‘Adaptive mechanisms in pathogens: Universal aneuploidy in *Leishmania*’, *Trends Parasitol.* **28**(9), 370–376.
- [37] Möller, M., Habig, M., Freitag, M. and Stukenbrock, E. H. 2018, ‘Extraordinary genome instability and widespread chromosome rearrangements during vegetative growth’, *Genetics* **210**(2), 517–529.
- [38] Naylor, R. M. and van Deursen, J. M. 2016, ‘Aneuploidy in cancer and aging’, *Annu. Rev. Genet.* **50**(1), 45–66.
- [39] Niwa, O., Tange, Y. and Kurabayashi, A. 2006, ‘Growth arrest and chromosome instability in aneuploid yeast’, *Yeast* **23**(13), 937–950.
- [40] Otto, S. P. and Day, T. 2007, *A biologist’s guide to mathematical modeling in ecology and evolution*, Princeton University Press.
- [41] Pavelka, N., Rancati, G., Zhu, J., Bradford, W. D., Saraf, A., Florens, L., Sanderson, B. W., Hattem, G. L. and Li, R. 2010, ‘Aneuploidy confers quantitative proteome changes and phenotypic variation in budding yeast.’, *Nature* **468**(7321), 321–5.
- [42] Peter, J., De Chiara, M., Friedrich, A., Yue, J. X., Pflieger, D., Bergström, A., Sigwalt, A., Barre, B., Freel, K., Llored, A., Cruaud, C., Labadie, K., Aury, J. M., Istace, B., Lebrigand, K., Barbry,

- 514 P., Engelen, S., Lemainque, A., Wincker, P., Liti, G. and Schacherer, J. 2018, ‘Genome evolution  
across 1,011 *Saccharomyces cerevisiae* isolates’, *Nature* **556**(7701), 339–344.
- 516 [43] Ram, Y., Dellus-Gur, E., Bibi, M., Karkare, K., Obolski, U., Feldman, M. W., Cooper, T. F.,  
Berman, J. and Hadany, L. 2019, ‘Predicting microbial growth in a mixed culture from growth  
518 curve data’, *Proceedings of the National Academy of Sciences* **116**(29), 14698–14707.
- 520 [44] Rancati, G., Pavelka, N., Fleharty, B., Noll, A., Trimble, R., Walton, K., Perera, A., Staehling-  
Hampton, K., Seidel, C. W. and Li, R. 2008, ‘Aneuploidy underlies rapid adaptive evolution of  
yeast cells deprived of a conserved cytokinesis motor’, *Cell* **135**(5), 879–893.
- 522 [45] Robbins, N., Caplan, T. and Cowen, L. E. 2017, ‘Molecular evolution of antifungal drug resis-  
tance’, *Annu. Rev. Microbiol.* **71**(1), 753–775.
- 524 [46] Robinson, D., Vanacloig-Pedros, E., Cai, R., Place, M., Hose, J. and Gasch, A. P. 2023, ‘Gene-  
by-environment interactions influence the fitness cost of gene copy-number variation in yeast’,  
526 *bioRxiv*.
- 528 [47] Rodrigues, M. L. and Albuquerque, P. C. 2018, ‘Searching for a change: The need for increased  
support for public health and research on fungal diseases’, *PLoS Negl. Trop. Dis.* **12**(6), 1–5.
- 530 [48] Rutledge, S. D., Douglas, T. A., Nicholson, J. M., Vila-Casadesús, M., Kantzler, C. L., Wangsa,  
D., Barroso-Vilares, M., Kale, S. D., Logarinho, E. and Cimini, D. 2016, ‘Selective advantage of  
trisomic human cells cultured in non-standard conditions’, *Scientific Reports* **6**(June 2015), 1–12.
- 532 [49] Santaguida, S. and Amon, A. 2015, ‘Short- and long-term effects of chromosome mis-segregation  
and aneuploidy’, *Nat. Rev. Mol. Cell Biol.* **16**(8), 473–485.
- 534 [50] Santaguida, S., Vasile, E., White, E. and Amon, A. 2015, ‘Aneuploidy-induced cellular stresses  
limit autophagic degradation’, *Genes Dev.* **29**(19), 2010–2021.
- 536 [51] Schvartzman, J. M., Sotillo, R. and Benezra, R. 2010, ‘Mitotic chromosomal instability and  
cancer: Mouse modelling of the human disease’, *Nat. Rev. Cancer* **10**(2), 102–115.
- 538 [52] Selmecki, A. M., Dulmage, K., Cowen, L. E., Anderson, J. B. and Berman, J. 2009, ‘Acquisition  
of aneuploidy provides increased fitness during the evolution of antifungal drug resistance’, *PLoS  
540 Genet.* **5**(10), e1000705.
- 542 [53] Selmecki, A. M., Forche, A. and Berman, J. 2010, ‘Genomic plasticity of the human fungal  
pathogen *Candida albicans*’, *Eukaryot. Cell* **9**(7), 991–1008.

- 544 [54] Selmecki, A. M., Gerami-Nejad, M., Paulson, C., Forche, A. and Berman, J. 2008, ‘An isochromosome confers drug resistance in vivo by amplification of two genes, erg11 and tac1’, *Mol. Microbiol.* **68**(3), 624–641.
- 546 [55] Sheltzer, J. M. and Amon, A. 2011, ‘The aneuploidy paradox: Costs and benefits of an incorrect karyotype’, *Trends Genet.* **27**(11), 446–453.
- 548 [56] Sheltzer, J. M., Blank, H. M., Pfau, S. J., Tange, Y., George, B. M., Humpton, T. J., Brito, I. L., Hiraoka, Y., Niwa, O. and Amon, A. 2011, ‘Aneuploidy drives genomic instability in yeast’, *Science* **333**(6045), 1026–1030.
- 552 [57] Sheltzer, J. M., Ko, J. H., Replogle, J. M., Habibe Burgos, N. C., Chung, E. S., Meehl, C. M., Sayles, N. M., Passerini, V., Storchova, Z. and Amon, A. 2017, ‘Single-chromosome gains commonly function as tumor suppressors’, *Cancer Cell* **31**(2), 240–255.
- 554 [58] Sionov, E., Lee, H., Chang, Y. C. and Kwon-Chung, K. J. 2010, ‘*Cryptococcus neoformans* overcomes stress of azole drugs by formation of disomy in specific multiple chromosomes’, *PLoS Pathog.* **6**(4), e1000848.
- 558 [59] Sisson, S. A., Fan, Y. and Tanaka, M. M. 2007, ‘Sequential monte carlo without likelihoods’, *Proceedings of the National Academy of Sciences* **104**(6), 1760–1765.
- 560 [60] Sonti, R. V. and Roth, J. R. 1989, ‘Role of gene duplications in the adaptation of *Salmonella typhimurium* to growth on limiting carbon sources.’, *Genetics* **123**(1), 19–28.
- 562 [61] Syga, S., David-Rus, D., Schälte, Y., Hatzikirou, H. and Deutsch, A. 2021, ‘Inferring the effect of interventions on covid-19 transmission networks’, *Scientific Reports* **11**(1), 1–11.
- 564 [62] Todd, R. T., Forche, A. and Selmecki, A. M. 2017, ‘Ploidy variation in fungi: Polyploidy, aneuploidy, and genome evolution’, *Microbiol. Spectr.* **5**(4), 1–20.
- 566 [63] Toni, T., Welch, D., Strelkowa, N., Ipsen, A. and Stumpf, M. P. 2009, ‘Approximate bayesian computation scheme for parameter inference and model selection in dynamical systems’, *J. R. Soc. Interface* **6**(31), 187–202.
- 568 [64] Torres, E. M., Dephoure, N., Panneerselvam, A., Tucker, C. M., Whittaker, C. A., Gygi, S. P., Dunham, M. J. and Amon, A. 2010, ‘Identification of aneuploidy-tolerating mutations’, *Cell* **143**(1), 71–83.
- [65] Torres, E. M., Sokolsky, T., Tucker, C. M., Chan, L. Y., Boselli, M., Dunham, M. J. and Amon,

- 572 A. 2007, ‘Effects of aneuploidy on cellular physiology and cell division in haploid yeast’, *Science* (80-. ). **317**(5840), 916–924.
- 574 [66] Tsai, H. J., Nelliat, A. R., Choudhury, M. I., Kucharavy, A., Bradford, W. D., Cook, M. E., Kim, J., Mair, D. B., Sun, S. X., Schatz, M. C. and Li, R. 2019, ‘Hypo-osmotic-like stress underlies  
576 general cellular defects of aneuploidy’, *Nature* .
- 578 [67] Williams, B. R., Prabhu, V. R., Hunter, K. E., Glazier, C. M., Whittaker, C. a., Housman,  
580 D. E. and Amon, A. 2008, ‘Aneuploidy affects proliferation and spontaneous immortalization in  
mammalian cells’, *Science* **322**(5902), 703–709.
- 582 [68] Yang, F., Todd, R. T., Selmecki, A., Jiang, Y. Y., Cao, Y. B. and Berman, J. 2021, ‘The fitness  
costs and benefits of trisomy of each *Candida albicans* chromosome’, *Genetics* **218**(2), 1–7.
- 584 [69] Yona, A. H., Frumkin, I. and Pilpel, Y. 2015, ‘A relay race on the evolutionary adaptation  
spectrum’, *Cell* **163**(3), 549–559.
- 586 [70] Yona, A. H., Manor, Y. S., Herbst, R. H., Romano, G. H., Mitchell, A., Kupiec, M., Pilpel, Y.  
and Dahan, O. 2012, ‘Chromosomal duplication is a transient evolutionary solution to stress.’,  
*Proceedings of the National Academy of Sciences* **109**(51), 21010–5.
- 588 [71] Zhu, J., Pavelka, N., Bradford, W. D., Rancati, G. and Li, R. 2012, ‘Karyotypic determinants of  
chromosome instability in aneuploid budding yeast’, *PLoS Genetics* **8**(5).
- 590 [72] Zhu, J., Tsai, H.-J., Gordon, M. R. and Li, R. 2018, ‘Cellular stress associated with aneuploidy’,  
*Dev. Cell* **44**(4), 420–431.
- 592 [73] Zhu, Y. O., Sherlock, G. and Petrov, D. A. 2016, ‘Whole genome analysis of 132 clinical *Sac-*  
*charomyces cerevisiae* strains reveals extensive ploidy variation’, *G3 Genes, Genomes, Genetics*  
**6**(8), 2421–2434.
- 594 [74] Zhu, Y. O., Siegal, M. L., Hall, D. W. and Petrov, D. A. 2014, ‘Precise estimates of mutation rate  
and spectrum in yeast’, *Proceedings of the National Academy of Sciences* **111**(22), E2310–E2318.

596 **Supplementary Material**

## Supplementary Analysis

598 **Sensitivity analysis.** Changing a single parameter while keeping the rest fixed at the MAP estimate produces a worse fit to the data (Figure S6). Furthermore, we fitted models with a mutation rate  
600 fixed at  $\mu = 10^{-5}$ ,  $10^{-6}$  and  $10^{-7}$ . We inferred similar parameters estimates for the model with  
 $\mu = 10^{-6}$  compared to the model with a free  $\mu$  parameter, in which the inferred mutation rate is  
602  $\mu \approx 3 \cdot 10^{-6}$ . Inference assuming  $\mu = 10^{-5}$  or  $\mu = 10^{-7}$  produced similar estimates except that the  
estimated aneuploidy rate,  $\delta$ , was higher, and assuming  $\mu = 10^{-7}$ , the estimated fitness of  $2n+1$  was  
604 lower (Figure S7).

**Extended informative prior distribution.** In an extended informative prior distribution, we used  
606 additional growth curves of  $2n^*$  (*refined* strain from Yona et al.<sup>70</sup>) and  $2n+1$  in 39 °C to estimate  
 $w_{2n^*}/w_{2n+1}$  (Figure S3H). The same distribution was used for  $w_{2n^*}/w_{2n+1*}$ . Thus, our main infor-  
608 mative prior uses a single prior distribution for fitness values of  $2n+1$ ,  $2n+1^*$ , and  $2n^*$ , whereas the  
extended informative prior uses one distribution for  $2n+1$ , and another distribution for both  $2n+1^*$   
610 and  $2n^*$ .

We estimated the parameters under this extended informative prior. Inference took much longer  
612 to run but the posterior distribution seemed to converge, as it did not change much in the final  
iterations. The posterior predictive plot shows that inference with this extended prior produces a  
614 posterior distribution that fails to explain the empirical observations (pink in Figure 3). However,  
the inferred posterior distribution is considerably narrower (compare Figures 2 and S8) and therefore  
616 parameter estimates are less variable. The estimated mutation rate was much lower compared to  
the main informative prior, with  $\mu = 2.474 \cdot 10^{-9}$  [ $2.423 \cdot 10^{-9} - 2.612 \cdot 10^{-9}$ ]. Other parameter  
618 estimates are:  $\delta = 2.705 \cdot 10^{-3}$  [ $2.094 \cdot 10^{-3} - 3.094 \cdot 10^{-3}$ ],  $w_{2n+1} = 1.022$  [ $1.021 - 1.024$ ],  
 $w_{2n+1*} = 1.052$  [ $1.05 - 1.054$ ],  $w_{2n^*} = 1.053$  [ $1.051 - 1.055$ ], the latter two being much higher  
620 compare to the main informative prior. Notably, the mode of the posterior ratio  $w_{2n^*}/w_{2n+1} = 1.0009$   
is much lower than the mode of the prior ratio of 1.033 (Figure S3H) and closer to the ratio of 1 that  
622 we assume in the main informative prior. Together with the posterior predictive results, we conclude  
that the main informative prior is preferable over the extended informative prior.

624 **Model with transitions to less-fit genotypes** We also estimated the parameters of a version of the  
model that includes transitions (mutation, chromosome loss and gain) to less-fit genotypes (e.g.,  $2n^*$

626 to  $2n+1^*$ ),

$$\begin{aligned}
 f_{2n}^m &= (1 - \delta - \mu)f_{2n}^s + \delta f_{2n+1}^s + \mu f_{2n^*}^s , \\
 f_{2n+1}^m &= \delta f_{2n}^s + (1 - \delta - \mu)f_{2n+1}^s + \mu f_{2n+1^*}^s , \\
 f_{2n+1^*}^m &= \mu f_{2n+1}^s + (1 - \delta - \mu)f_{2n+1^*}^s + \delta f_{2n^*}^s , \\
 f_{2n^*}^m &= \mu f_{2n}^s + \delta f_{2n+1^*}^s + (1 - \delta - \mu)f_{2n^*}^s .
 \end{aligned} \tag{7}$$

628 The inferred values are slightly different. The estimated mutation rate,  $\mu = 1.036 \cdot 10^{-7}$  [ $8.01 \cdot 10^{-8} - 1.339 \cdot 10^{-7}$ ], corresponds to a mutation target size of  $\sim 300 - 500$ , assuming the mutation  
 630 rate per base pair is roughly  $2 \cdot 10^{-10}$  (ref.<sup>74</sup>) or  $3.3 \cdot 10^{-10}$  (ref.<sup>35</sup>). The estimated aneuploidy  
 632 rate,  $\delta = 2.358 \cdot 10^{-4}$  [ $1.766 \cdot 10^{-4} - 2.837 \cdot 10^{-4}$ ] is 5-35-fold higher than in previous studies:  
 634 for Chromosome III in diploid *S. cerevisiae*, Zhu et al.<sup>74</sup> estimated  $6.7 \cdot 10^{-6}$  chromosome gain  
 events per generation, and Kumaran et al.<sup>32</sup> estimate  $3.0 - 4.3 \cdot 10^{-5}$  chromosome loss events per  
 636 generation (95% confidence interval). The estimated fitness values are  $w_{2n+1} = 1.024$  [ $1.023 - 1.025$ ],  
 638  $w_{2n+1^*} = 1.025$  [ $1.024 - 1.026$ ],  $w_{2n^*} = 1.032$  [ $1.031 - 1.033$ ], all relative to the fitness of  $2n$ , which  
 is set to  $w_{2n} = 1$ . Thus, we can infer that the cost of trisomy is  $c = w_{2n^*} - w_{2n+1^*} = 0.007$  (or 0.7%)  
 and the benefit of trisomy is  $w_{2n+1} - 1 - c = 0.017$  (1.7%), whereas the benefit of beneficial mutation  
 is  $w_{2n^*} - 1 = 0.032$  (3.2%).

We simulated genotype frequency dynamics using parameter samples from the posterior distribution,  
 640 and computed the posterior distribution of  $F_A$ . The mean  $F_A$  in this case is just 0.0189 [0.0004 -  
 642 0.1214 95% CI], lower than without the transitions to less-fit genotypes. Here,  $F_A$  is the sum of  
 frequencies of both  $2n_A^*$  and  $2n + 1_A^*$ , which reaches a frequency of 0.0007. Out of 100,000 posterior  
 samples, none had  $F_A$  above 0.05 (i.e., 5% of the population).

644 **Supplementary Figures & Tables**

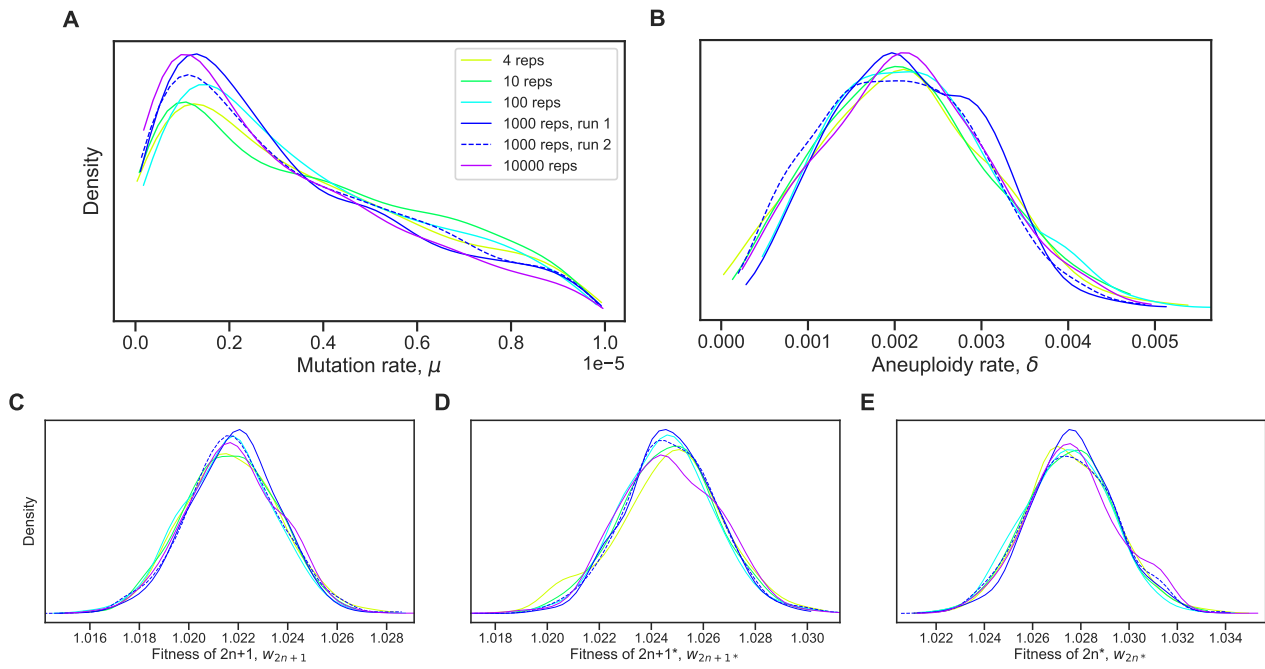


**Figure S1: Posterior distribution validation.** The posterior distribution of model parameters is roughly the same regardless of the number of simulations (4-10,000 replicates) used to approximate the likelihood (eq. (4)).

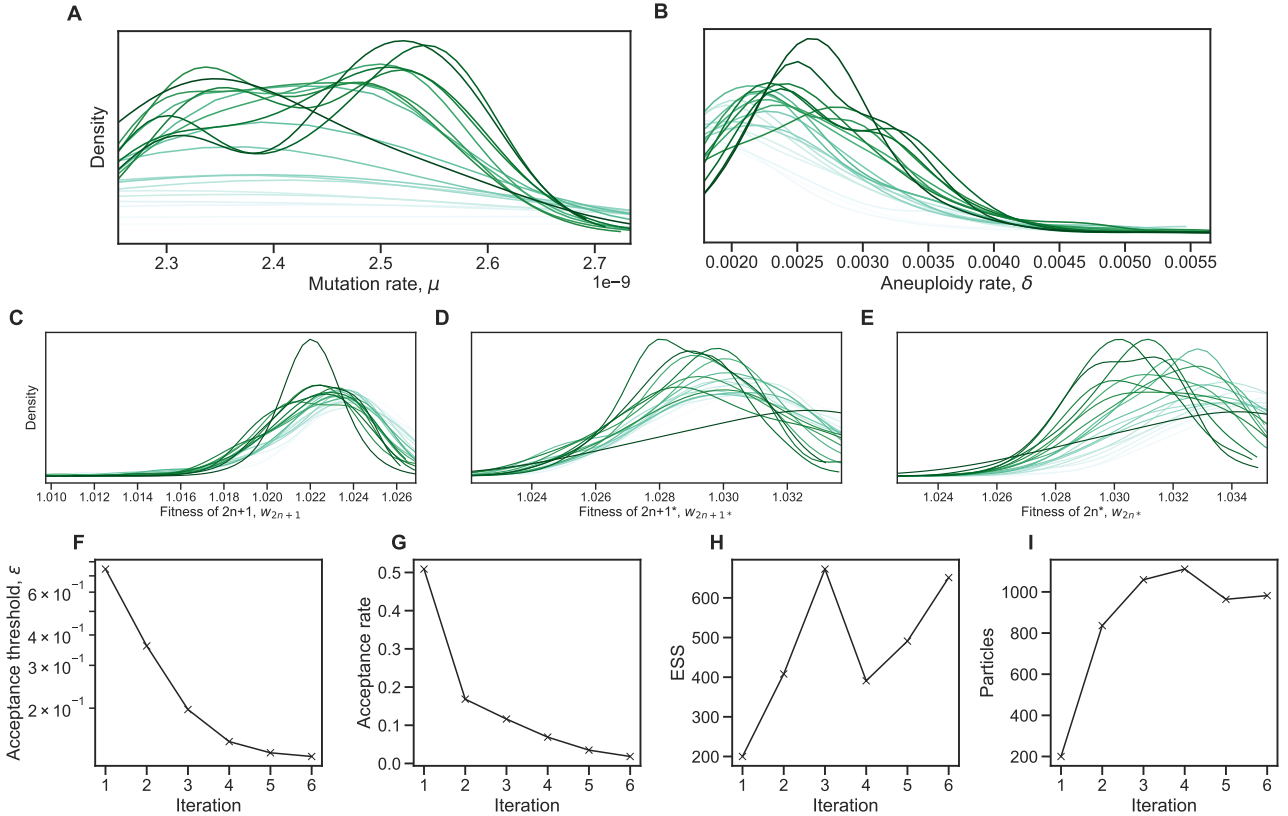


**Figure S2: Inference convergence.** The ABC-SMC algorithm was used to infer the model parameters. **(A-E)** The approximate posterior distributions of model parameters at each iteration of the ABC-SMC algorithm demonstrates convergence, as the posterior did not significantly change after the first iteration,  $t = 1$ . **(F-I)** ABC-SMC measures of convergence. After iteration number 6, the acceptance threshold was  $\epsilon = 0.13$  (i.e.,  $\mathcal{L} = 0.87$ , eq. (4)), the acceptance rate was 0.018, the number of particles was 982, and the effective sample size ESS=651.

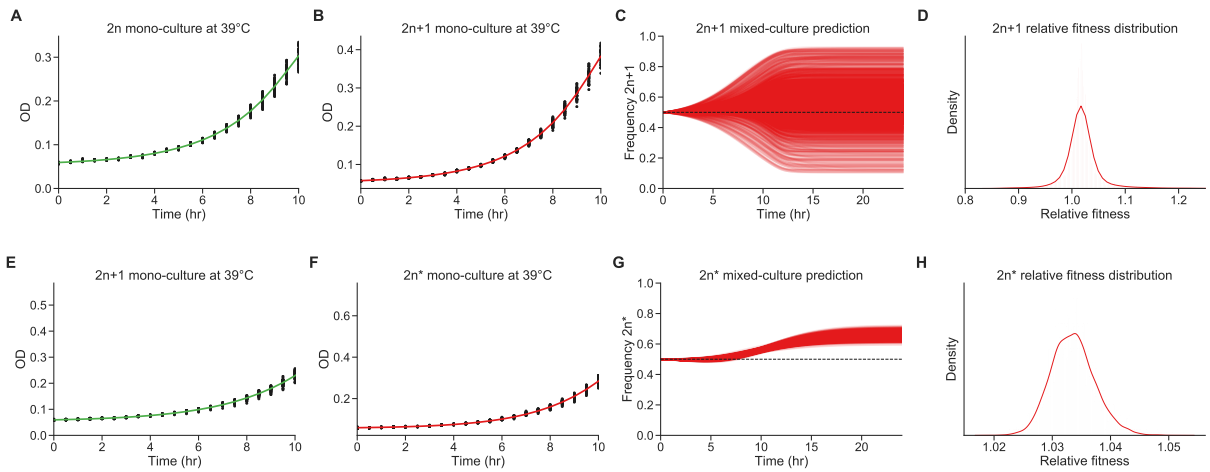


**Figure S3: Fitness estimation from growth curves.** **(A-D)** Fitness estimation from growth curves of  $2n$  and  $2n+1$  at  $39^{\circ}\text{C}$ .  $w_{2n+1}/w_{2n}=1.024$  (95% CI: 0.959 - 1.115). **Curveball (E-H)** Fitness estimation from growth curves of  $2n+1$  and  $2n^*$  at  $39^{\circ}\text{C}$ .  $w_{2n^*}/w_{2n+1}=1.033$  (95% CI: 1.027 - 1.041). Growth curves previously described in Yona et al.<sup>70</sup>, Figs. 3C, 4A, and S2. Fitness estimated from growth curves using Curveball, a method for predicting results of competition experiments from growth curve data<sup>43</sup> [curveball.yoavram.com](http://curveball.yoavram.com). See *Models and Methods, Prior distributions* for more details. **(A,B;E,F)** Mono-culture growth curve data (markers) and best-fit growth models (lines). **(C,G)** The mixed-culture prediction for the strains from A,B and E,F respectively, 6,375 generated curves. **(D,H)** The relative fitness distribution for  $2n+1$  relative to  $2n$  (panel D) and  $2n^*$  relative to  $2n+1$  (panel H). Figures generated by Curveball.

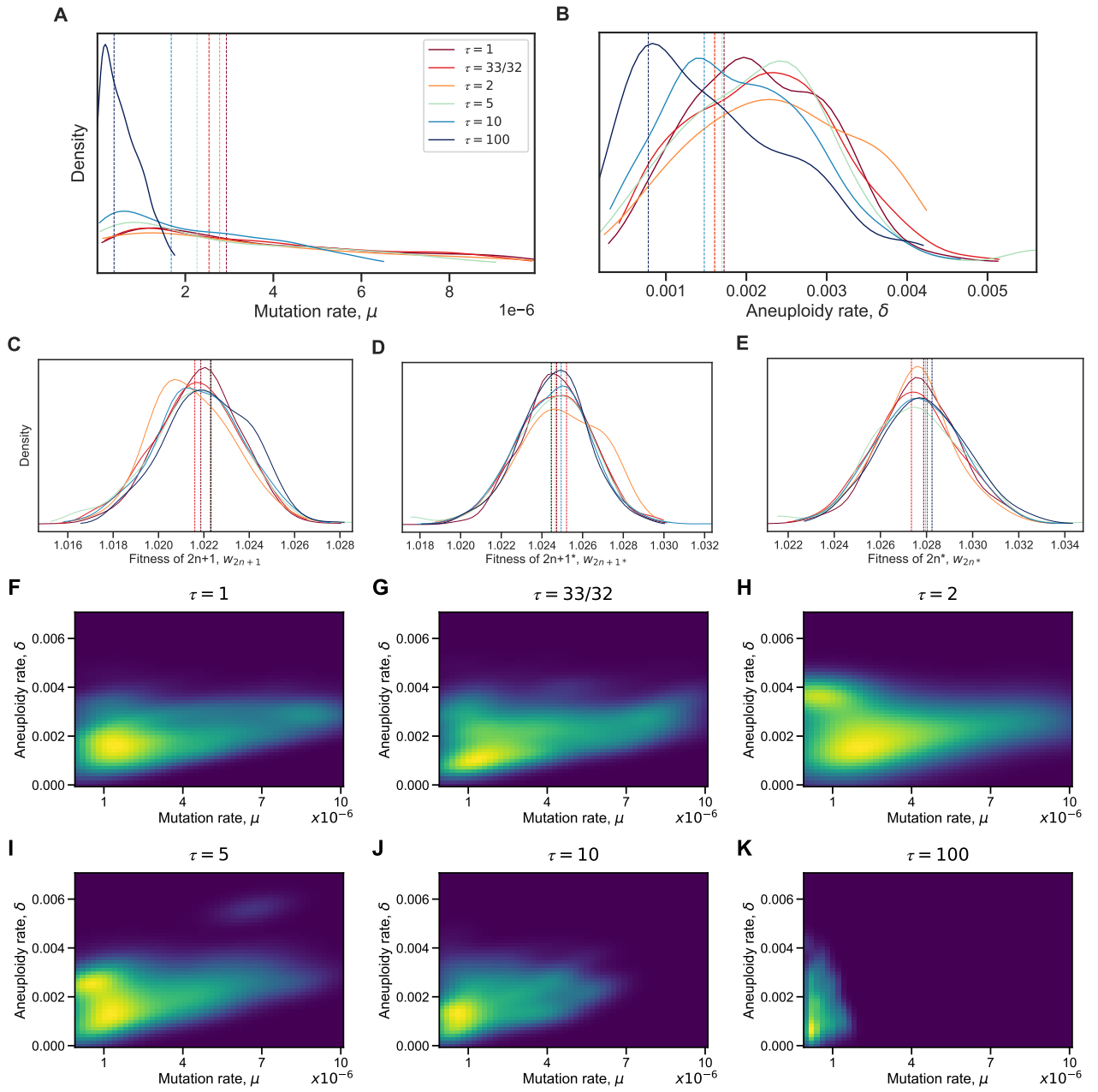


**Figure S4: Model with elevated mutation rate in aneuploid cells.** (A-E) The inferred posterior distributions for models with different values of  $\tau$ , the fold-increase in mutation rate in aneuploid cells ( $2n+1$  and  $2n+1^*$ ). Vertical dashed lines represent the MAP (maximum a posteriori) of each distribution. When the increase in mutation rate is high,  $\tau = 10$  and  $\tau = 100$ , the inferred mutation (A) and aneuploidy (B) rates tend to be lower. (F-K) The inferred joint posterior distribution of mutation rate ( $\mu$ ) and aneuploidy rate ( $\delta$ ) with different  $\tau$  values (dark purple and bright yellow for low and high density, respectively).

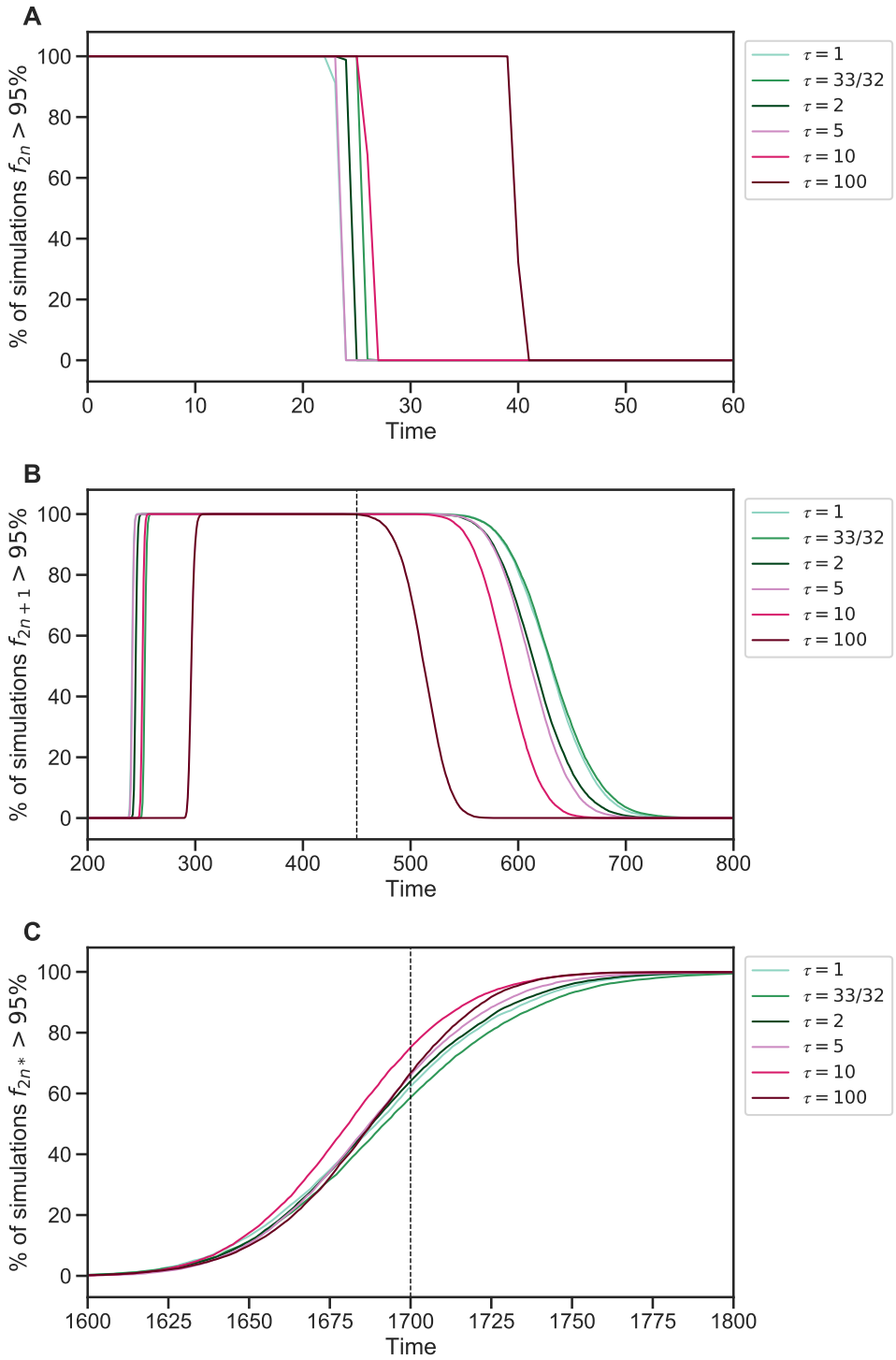


**Figure S5: Genotype fixations for models with increased genetic instability.** We estimated the parameters for different models, each assuming a different value of  $\tau$ , the fold-increase in mutation rate in aneuploid cells. We then generated 10,000 simulations using the MAP estimate of each model and evaluated the fraction of simulations in which the frequency of genotype  $2n$  (**A**),  $2n+1$  (**B**), and  $2n^*$  (**C**) is above 95% (y-axis) at each generation (x-axis). Note that  $2n+1^*$  did not fix. We can see that  $\tau = 100$  can be distinguished if the waiting time for  $f_{2n} < 95\%$  is known (panel A) or if the waiting time for  $f_{2n+1} > 95\%$  or  $f_{2n+1} < 95\%$  is known (panel B). It is harder to distinguish between  $1 \leq \tau \leq 10$ .

**Table S1: WAIC values for different  $\tau$  values.** Differences of less than 6 are considered of weak significance<sup>26</sup>.

Model	WAIC
$\tau = 1$	-9
$\tau = 33/32$	-9
$\tau = 2$	-8
$\tau = 5$	-12
$\tau = 10$	-9
$\tau = 100$	-12

WAIC defined in eq. (6).

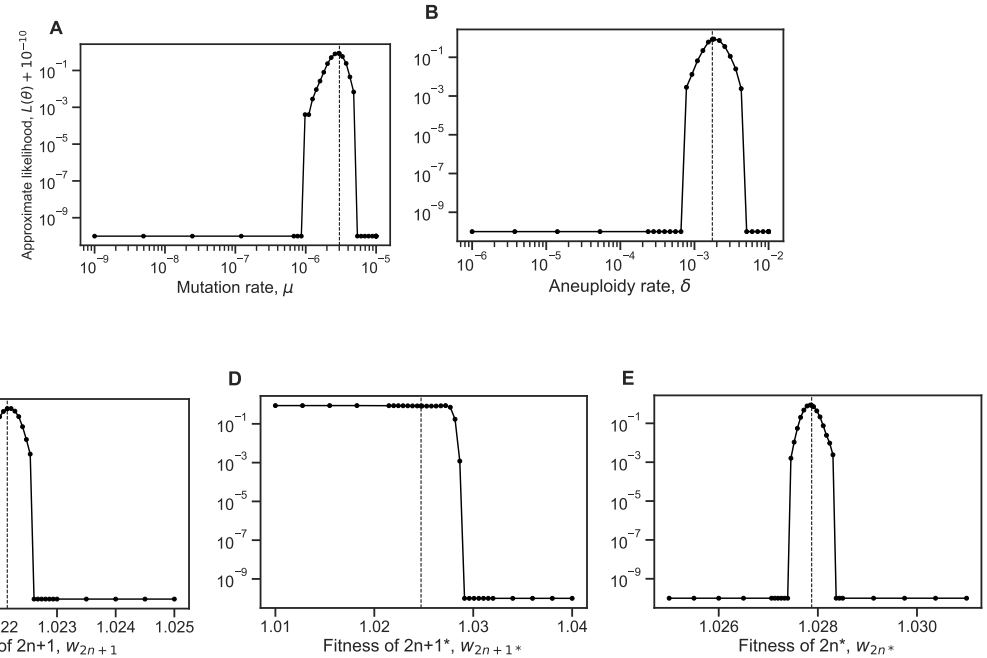


**Figure S6: Likelihood profiles.** Sensitivity of the model approximate likelihood,  $\mathcal{L}(\theta)$ , to changing a single parameter while the other parameters remain fixed at their MAP estimates. Dashed vertical line represents the MAP value. The prior distributions for the mutation rate and aneuploidy rate are  $\mu \sim U(10^{-9}, 10^{-5})$  and  $\delta \sim U(10^{-6}, 10^{-2})$ , respectively.

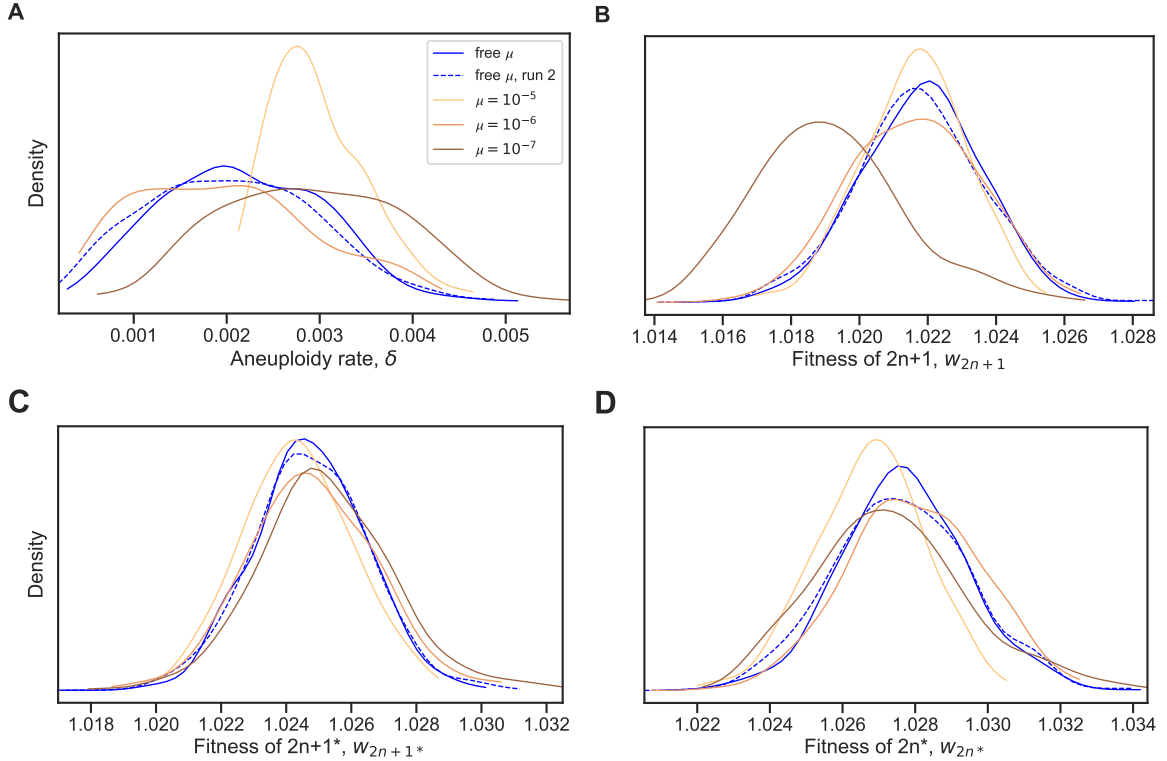


**Figure S7: Model with fixed mutation rate.** (A-D) The inferred posterior distributions for models with free and fixed mutation rate,  $\mu$ . The MAP (maximum a posteriori) and 50% HDI (highest density interval) for each model are: **free  $\mu$ , run 1:**  $\delta = 1.720 \cdot 10^{-3}$  [ $1.470 \cdot 10^{-3} - 2.786 \cdot 10^{-3}$ ],  $w_{2n+1} = 1.022$  [1.021 – 1.023],  $w_{2n+1^*} = 1.025$  [1.024 – 1.026],  $w_{2n^*} = 1.028$  [1.026 – 1.029]; **free  $\mu$ , run 2:**  $\delta = 2.129 \cdot 10^{-3}$  [ $1.334 \cdot 10^{-3} - 2.695 \cdot 10^{-3}$ ],  $w_{2n+1} = 1.022$  [1.02 – 1.023],  $w_{2n+1^*} = 1.025$  [1.023 – 1.026],  $w_{2n^*} = 1.028$  [1.026 – 1.029];  **$\mu = 10^{-5}$ :**  $\delta = 2.903 \cdot 10^{-3}$  [ $2.399 \cdot 10^{-3} - 3.156 \cdot 10^{-3}$ ],  $w_{2n+1} = 1.022$  [1.021 – 1.023],  $w_{2n+1^*} = 1.024$  [1.023 – 1.025],  $w_{2n^*} = 1.027$  [1.026 – 1.028];  **$\mu = 10^{-6}$ :**  $\delta = 1.917 \cdot 10^{-3}$  [ $9.624 \cdot 10^{-4} - 2.447 \cdot 10^{-3}$ ],  $w_{2n+1} = 1.022$  [1.02 – 1.023],  $w_{2n+1^*} = 1.025$  [1.023 – 1.026],  $w_{2n^*} = 1.028$  [1.027 – 1.029];  **$\mu = 10^{-7}$ :**  $\delta = 2.901 \cdot 10^{-3}$  [ $2.139 \cdot 10^{-3} - 3.671 \cdot 10^{-3}$ ],  $w_{2n+1} = 1.019$  [1.017 – 1.02],  $w_{2n+1^*} = 1.025$  [1.024 – 1.026],  $w_{2n^*} = 1.027$  [1.026 – 1.029].

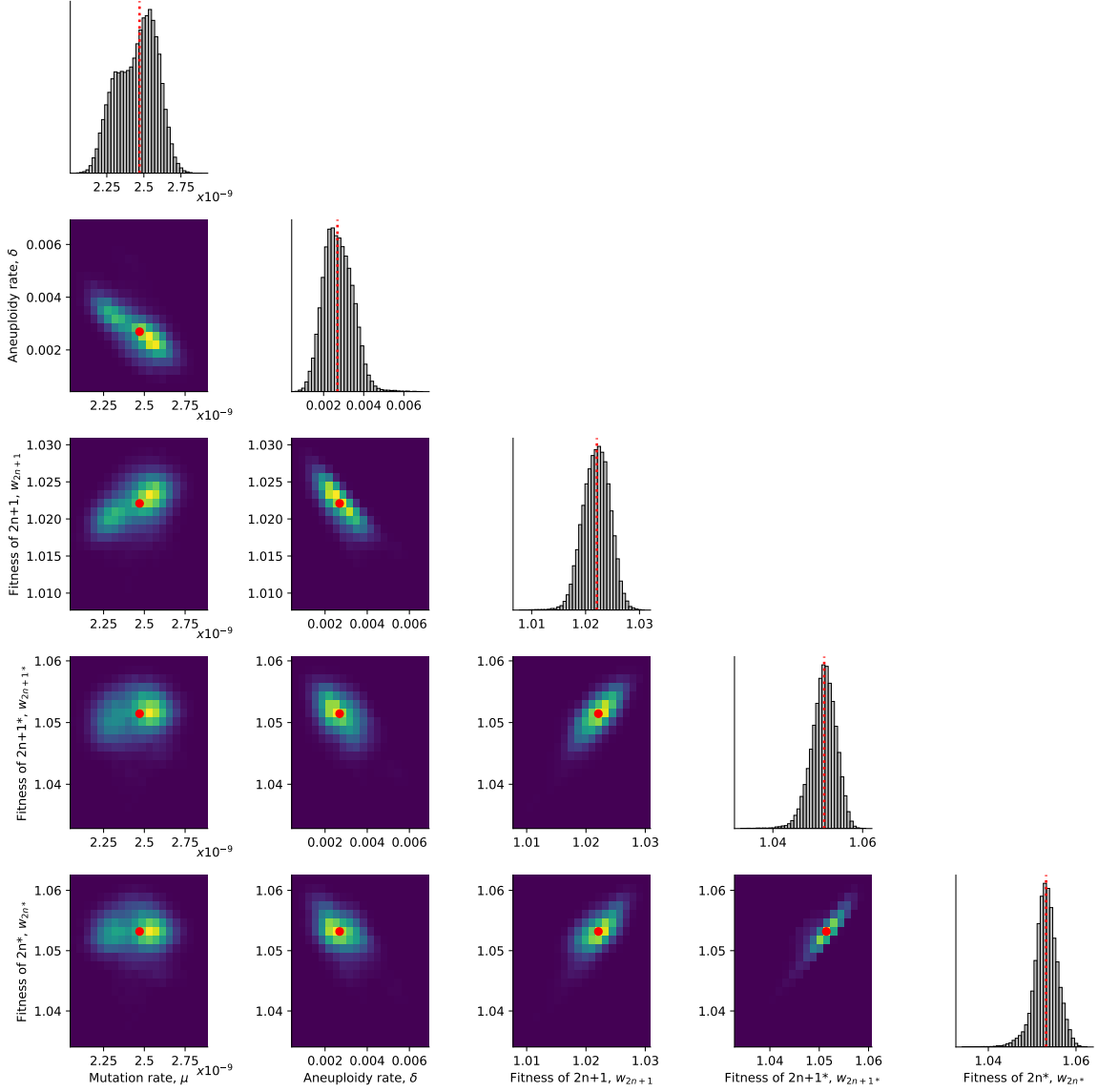


**Figure S8: Posterior distribution of parameters inferred with the extended prior distribution.** On the diagonal, the inferred posterior distribution of each model parameter. Below the diagonal, the inferred joint posterior distribution of pairs of model parameters (dark purple and bright yellow for low and high density, respectively). Red markers and orange lines for the joint MAP estimate (which may differ from the marginal MAP, as the marginal distribution integrates over all other parameters).

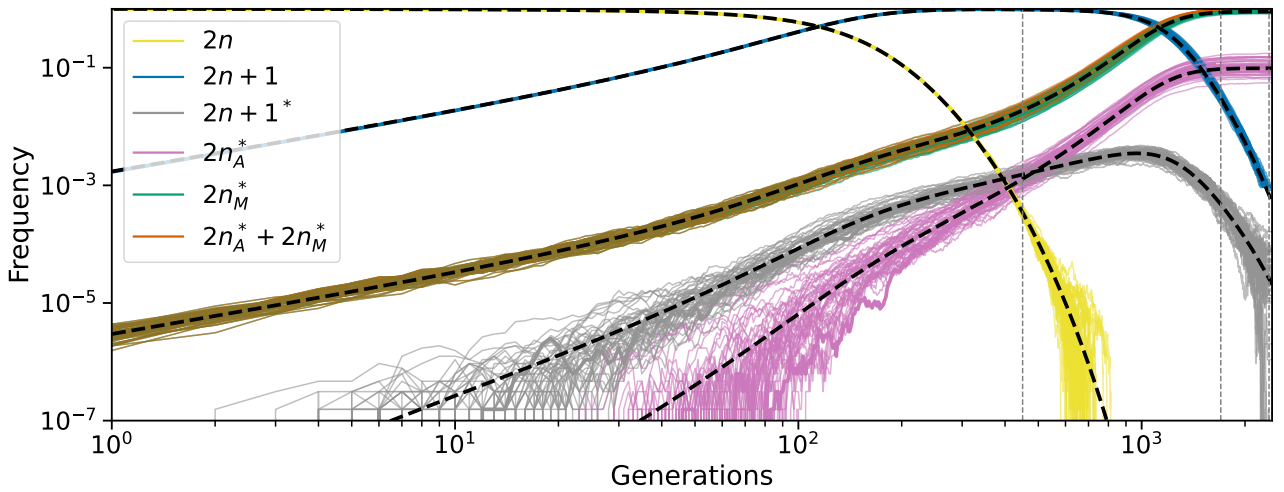


**Figure S9: Posterior predicted genotype frequencies in log-log scale.** Frequency dynamics of the different genotypes with MAP parameter estimates, same as Figure 4A, but in log-log scale. Black dashed curves for a deterministic model without genetic drift. Clearly, appearance of  $2n+1$  and  $2n_M^*$  is deterministic. Appearance of  $2n+1^*$ , and therefore  $2n_A^*$ , is stochastic, however, the frequency dynamics are deterministic above a frequency of roughly 0.001. Note that the  $2n_M^*$  and the  $2n_A^* + 2n_M^*$  lines are overlapping for much of their trajectories.

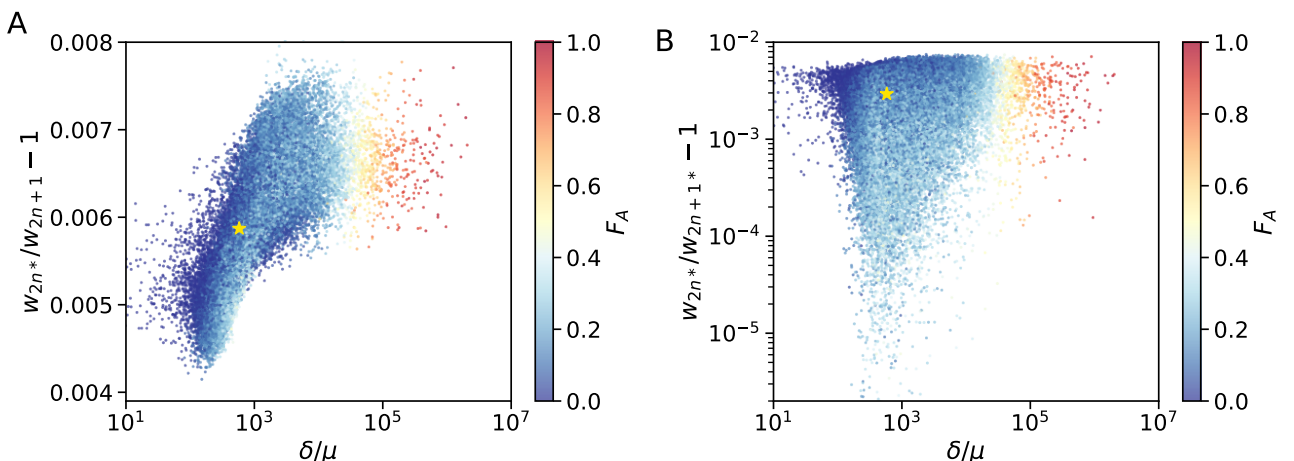


**Figure S10: Posterior distribution of  $F_A$ .** (A,B)  $F_A$  values (color coded) as in Figure 4 for different parameter choices on the x- and y-axes. White star denotes the MAP estimate.